Molecular Biology of the Cell
Vol. 18, 3323–3339, September 2007

Distinct Domains of Yeast Cortical Tag Proteins Bud8p and Bud9p Confer Polar Localization and Functionality[D]

Anne-Brit Krappmann,* Naimeh Taheri,†‡ Melanie Heinrich,* and Hans-Ulrich Mösch*

*Department of Genetics, Philipps-University, D-35032 Marburg, Germany; and †Institute for Microbiology and Genetics, Georg-August University, D-37077 Göttingen, Germany

Submitted October 6, 2006; Revised June 5, 2007; Accepted June 12, 2007
Monitoring Editor: Daniel Lew

In *Saccharomyces cerevisiae*, diploid yeast cells follow a bipolar budding program, which depends on the two transmembrane glycoproteins Bud8p and Bud9p that potentially act as cortical tags to mark the cell poles. Here, we have performed systematic structure-function analyses of Bud8p and Bud9p to identify functional domains. We find that polar transport of Bud8p and Bud9p does not depend on N-terminal sequences but instead on sequences in the median part of the proteins and on the C-terminal parts that contain the transmembrane domains. We show that the guanosine diphosphate (GDP)/guanosine triphosphate (GTP) exchange factor Bud5p, which is essential for bud site selection and physically interacts with Bud8p, also interacts with Bud9p. Regions of Bud8p and Bud9p predicted to reside in the extracellular space are likely to confer interaction with the N-terminal region of Bud5p, implicating indirect interactions between the cortical tags and the GDP/GTP exchange factor. Finally, we have identified regions of Bud8p and Bud9p that are required for interaction with the cortical tag protein Rax1p. In summary, our study suggests that Bud8p and Bud9p carry distinct domains for delivery of the proteins to the cell poles, for interaction with the general budding machinery and for association with other cortical tag proteins.

INTRODUCTION

The budding yeast *Saccharomyces cerevisiae* is a useful model system to study various aspects of cell polarization (Chant, 1999; Pruyne and Bretscher, 2000a). Establishment of yeast cell polarity can be divided into three basic steps (Drubin and Nelson, 1996; Pruyne and Bretscher, 2000b). In the first step, cells choose a site on their cell surface, a spatial landmark, toward which they will polarize. In the second step, the landmark is recognized by a number of proteins that are collectively called polarity establishment proteins or actin-organizing complex. In the final step, this complex of proteins recruits the machinery that organizes and polymerizes actin, actin-associated proteins, and septins to the selected site of growth. As a consequence, internal membranes and other factors can be transported along the polarized cytoskeleton toward the landmark, leading to directed cell division and polarized growth. Yeast cells must choose the site for bud initiation at the beginning of every round of cell division. This process follows specific spatial patterns that are under genetic control of the corresponding cell type (Freifelder, 1960; Hicks *et al*., 1977; Chant and Pringle, 1995). Haploid cells bud in an axial pattern, where mother and daughter cell bud adjacent to the cell pole that defined the previous mother-daughter junction. This region of the yeast surface is also termed the proximal pole or the birth end of the cell. Diploid yeast cells bud in a bipolar pattern, where buds are formed either at the proximal pole or at the site opposite to it, called the distal pole. Genetic analysis has identified a large number of genes that are involved in the process of bud site selection, which initially have been classified according to their loss-of-function phenotype. One class of genes is specifically required for axial budding of haploid cells without affecting the bipolar budding pattern of diploids, and this class includes *BUD3*, *BUD4*, *AXL2/BUD10*, and *AXL1* (Fujita *et al*., 1994). Bud3p, Bud4p, and Axl2p/Bud10p together with septins seems to constitute a transient landmark that is deposited at the mother-bud neck during each cell cycle (Sanders and Herskowitz, 1996; Lord *et al*., 2000). A second class of genes is required for both axial and bipolar budding, and this class includes *RSR1/BUD1*, *BUD2*, and *BUD5* (Chant and Herskowitz, 1991). Mutations in these genes cause random budding patterns in both haploid and diploid cells. Rsr1p/Bud1p, Bud2p, and Bud5p constitute a GTPase signaling module that is thought to help in directing bud formation components to the site of cell division by interaction with the spatial landmark (Park *et al*., 1997, 1999). A third class of >100 genes is required for the bipolar pattern of diploid yeast but not for the axial pattern. Mutations in these genes either shift the bud site selection of diploid cells from bipolar to unipolar (with bias to either the distal or the proximal pole) or cause random budding (Bauer *et al*., 1993; Zahner *et al*., 1996; Mösch and Fink, 1997; Sheu *et al*., 2000; Ni and Snyder, 2001).

Bud8p and Bud9p are two transmembrane glycoproteins that are thought to act as landmark components or cortical tags for the bipolar budding program of diploid cells

This article was published online ahead of print in *MBC in Press* (http://www.molbiolcell.org/cgi/doi/10.1091/mbc.E06–10–0899) on June 20, 2007.

[D] The online version of this article contains supplemental material at *MBC Online* (http://www.molbiolcell.org).

‡ Present address: Department of Molecular Genetics, The Ohio State University, Columbus, OH 43210-1292.

Address correspondence to: Hans-Ulrich Mösch (moesch@staff.uni-marburg.de).

© 2007 by The American Society for Cell Biology

(Zahner *et al*., 1996; Taheri *et al*., 2000; Harkins *et al*., 2001). Bud8p is localized at the distal cell pole, and it is required for distal bud site selection, suggesting that it is part of the distal landmark. Bud9p is localized at the proximal pole, and it is required for proximal pole selection, indicating that it functions as part of the proximal tag (Harkins *et al*., 2001). Because Bud9p in certain strain backgrounds is also found at the distal pole and physically interacts with Bud8p, it might fulfill an additional function at the distal pole where it seems to act as a nutritionally controlled inhibitor of distal budding (Taheri *et al*., 2000). Bud8p and Bud9p interact with two further integral membrane proteins required for bipolar budding, Rax1p and Rax2p, indicating that interactions among these proteins are important to mark cortical sites (Chen *et al*., 2000; Kang *et al*., 2004a). In addition, a physical link has been established between Bud8p and Bud5p, suggesting that Bud8p might control bud site selection by interaction with the Rsr1p/Bud1p GTPase module (Kang *et al*., 2004b). The molecular functions of Bud8p and Bud9p are not well understood. The overall structures of Bud8p and Bud9p are similar in that both are predicted to consist of a large N-terminal extracellular domain, followed by a membrane-spanning domain (TM1), a short cytoplasmic loop, a second membrane-spanning domain (TM2), and a very short extracellular domain at the C terminus. The N-terminal portion of both proteins contains several potential *N*- and *O*-glycosylation sites that seem to be functional (Harkins *et al*., 2001). However, domains of Bud8p and Bud9p that are required for transport of the proteins to the cell poles or that confer interaction with other landmark proteins or downstream-acting components of the budding machinery are not known. Here, we have performed a systematic analysis of Bud8p and Bud9p to better understand the structure and function of bipolar landmark proteins.

MATERIALS AND METHODS

Yeast Strains and Growth Conditions

Yeast strains used in this study are all congenic to the Σ1278b genetic background, and they are listed in Table 1. Standard methods for transformation and genetic crosses were used and standard yeast culture YPD, YNB, and SC media were prepared essentially as described previously (Guthrie and Fink, 1991). The *bud8*Δ*::HIS3* and *bud9*Δ*::HIS3* deletion mutations were introduced into haploid strains as described previously (Taheri *et al*., 2000), and YHUM829, YHUM861, YHUM904, YHUM994, YHUM995, YHUM1024, and YHUM1030 were obtained by appropriate genetic crosses. Homozygous diploid *BUD8* deletion strains YHUM842 to YHUM856 were obtained by integration of single copies of plasmids BHUM782 to BHUM794 (after linearization with StuI) at the *URA3*-locus of *bud8*Δ strains YHUM861 and YHUM904, respectively, and appropriate crossing of resulting haploid strains. Heterozygous *BUD8* deletion strains YHUM1023 to YHUM1028 were obtained by crossing appropriate haploid *BUD8* deletion strains to strain YHUM217 carrying a functional *BUD8* gene. Homozygous diploid *BUD9* deletion strains YHUM1009 to YHUM1022 were obtained by integration of single copies of plasmids BHUM796 to BHUM809 (after linearization with Bst1107I) at the *TRP1*-locus of *bud9*Δ strain YHUM994 and of plasmids BHUM810 to BHUM823 (after linearization with BstEII) at the *LEU2*-locus of *bud9*Δ strain YHUM995, respectively, and appropriate crossing of resulting haploid strains. Heterozygous *BUD9* deletion strains YHUM1029 to YHUM1031 were obtained by crossing appropriate haploid *BUD9* deletion strains to strain YHUM215 carrying a functional *BUD9* gene. In all cases, single plasmid integration was verified by southern hybridization analysis. Strains expressing *BUD5-GFP* were constructed by direct tagging of the endogenous *BUD5* gene (Sheff and Thorn, 2004) in haploid strains followed by crossing to obtain corresponding diploid strains.

Plasmids

BUD8. To generate plasmids BHUM782 to BHUM794 (Table 2), a polymerase chain reaction (PCR) strategy was used (oligonucleotide primers are described in Supplemental Material). In the first step, six fragments were generated by PCR by using the oligonucleotides T3 and BUD8DEL01 to BUD8DEL06, respectively, and plasmid pME1775 (Taheri *et al*., 2000) carrying a sixfold myc epitope-tagged version of *BUD8* as template. The resulting fragments made up 924 base pairs of upstream sequence and different parts of the *BUD8* open reading frame (ORF) followed by a BglII restriction site at the 3′ end. Another six fragments making up different parts of the *BUD8* ORF and 588 or 712 base pairs of the downstream sequence were amplified using primers BUD8DEL07 to BUD8DEL12 together with BUD8X-6 or BUD8DEL13, respectively. These fragments contain a BglII site at their 5′ end. Fragments of both groups were subcloned into pBlueskript KS after digestion with NotI/BglII or BglII/XhoI, respectively, and they were verified by DNA sequencing using the ABI Prism Big Dye terminator sequencing kit and an ABI Prism 310 Genetic Analyzer (Applied Biosystems, Weiterstadt, Germany). Different combinations of fragments from both groups were joined together using the BglII restriction site. Resulting *BUD8* deletion constructs were inserted as NotI-XhoI fragments into pRS306 to obtain plasmids BHUM782 to BHUM793. Plasmid BHUM794 was constructed by a similar strategy, but fragments were joined using an XhoI restriction site that was introduced instead of a BglII site. The different *BUD8* deletion constructs were further subcloned as NotI-XhoI fragments into pRS425 to obtain plasmids BHUM723, BHUM706, and BHUM1016 to BHUM1025 as well as into pRS426 to obtain plasmids BHUM867 to BHUM879.

For generation of plasmids BHUM825 and BHUM826, a GFP_{UV}-*BUD8* DNA fragment making up 924 base pairs of upstream sequence, the *BUD8* start codon, 720 base pairs of GFP_{UV}-coding sequence, 15 base pairs of the *BUD8* ORF, and an incomplete BglII site (5′-GATCT-3′) was generated by PCR by using primers T3 and BUD8DEL01-P and plasmid pME1771 (Taheri *et al*., 2000) as template. The resulting PCR product was digested with NotI and cloned into plasmids BHUM868 and BHUM869, respectively, that had been digested with BglII, treated with mung bean nuclease to remove single-stranded ends, and then digested with NotI. Plasmids BHUM824 and BHUM828 to BHUM836 were obtained by gap repair in yeast. First, a GFP_{UV}-*BUD8* fragment making up 356 base pairs of upstream sequences followed by the *BUD8* start codon, 720 base pairs of the GFP_{UV}-coding sequence, and 208 base pairs of the *BUD8* ORF was amplified by PCR by using oligonucleotides AO-BUD8-1 and AO-BUD8-2 and plasmid pME1771 (Taheri *et al*., 2000) as template. The resulting PCR product was inserted into EcoRV-digested pBlueskript KS and analyzed by DNA sequencing using oligonucleotides T3-I and T7-I. The GFP_{UV}-*BUD8* PCR product was further cotransformed into yeast strain RH2449 together with either of the plasmids BHUM867 or BHUM870 to BHUM879, respectively, which had been digested with NruI and dephosphorylated with alkaline shrimp phosphatase. Plasmid DNA was isolated from Ura^+ transformants and analyzed for the presence of a 700-base pair fragment containing the GFP_{UV}-tag by PCR by using primers AO-FP-1-1 and AO-FP-1-2. Correct plasmids were further verified by DNA sequencing and named BHUM824 and BHUM828 to BHUM836, respectively.

BUD9. Plasmids BHUM796 to BHUM823 were obtained by a similar strategy described for the *BUD8* deletion plasmids. Seven fragments containing parts of the *BUD9* ORF plus 944 base pairs of upstream sequence were generated by PCR by using plasmid BHUM795 as template and oligonucleotides BUD9X-1 and BUD9DEL01 to BUD9DEL07, respectively, that introduce a SpeI restriction site at the 5′ end and an EcoRI site at the 3′ end of the PCR products. In addition, the complete *BUD9* coding was amplified as SpeI-XhoI fragment with BUD9X-1 and BUD9Y-1. All fragments were inserted into plasmid pBlueskript KS, and a BglII fragment carrying a myc^9 epitope was isolated from plasmid BHUM894 and inserted into the single BglII site present after the start codon of the *BUD9* ORF present in all fragments. Another seven fragments making up parts of the *BUD9* ORF and 384 base pairs of the downstream region were amplified as EcoRI-XhoI fragments by using the oligonucleotides BUD9DEL08 to BUD9DEL14 and BUD9Y-1 and inserted into pBlueskript KS after digestion with EcoRI and XhoI. Sequencing confirmed the cloning of each PCR product and the correct orientation of the myc^9-epitopes in the SpeI-EcoRI fragments and the full-length version of *BUD9*. Appropriate fragments were combined using the EcoRI restriction site and subsequently cloned as SpeI-XhoI fragments into pRS304 to obtain plasmids BHUM796 to BHUM809, into pRS305 to obtain plasmids BHUM810 to BHUM823, into plasmid pRS425 to obtain plasmids BHUM1027 to BHUM1040 and into pRS426 to yield plasmids BHUM880 to BHUM893.

To generate plasmids BHUM838 and BHUM839, a *YFP-BUD9* DNA fragment making up 944 base pairs of upstream sequence, the *BUD9* start codon, 705 base pairs of yellow fluorescent protein (YFP)-coding sequence, and 18 base pairs of the *BUD9* ORF was amplified from BHUM895 by PCR by using oligonucleotides BUD9X-1 and BUD9DEL01. The fragment was digested with SpeI and EcoRI, inserted into pBlueskript KS, and verified DNA by sequencing. The SpeI-EcoRI fragment was then inserted into plasmid BHUM881 and BHUM882 after restriction with SpeI and EcoRI to yield plasmids BHUM838 and BHUM839. Plasmids BHUM837 and BHUM841 to BHUM850 were obtained by gap repair in yeast. First, an *YFP-BUD9* fragment was amplified by PCR by using BHUM895 as DNA template and primers AO-BUD9-1 and AO-BUD9-2. The resulting PCR product was verified by DNA sequencing after insertion into the EcoRV site of pBlueskript KS. In a second step, plasmids BHUM880 and BHUM884 to BHUM893 were linearized by digestion with BamHI, dephosphorylated with alkaline shrimp phosphatase and cotransformed into yeast strain RH2450 along with the PCR product carrying

Table 1. Yeast strains

Strain	Genotype	Source
RH2448	**a**/α *rsr1Δ::kanR/rsr1::kanR ura3-52/ura3-52 leu2::hisG/LEU2 trp1::hisG/TRP1*	Taheri *et al.* (2000)
RH2449	**a**/α *bud8Δ::HIS3/bud8Δ::HIS3 ura3-52/ura3-52 his3::hisG/his3::hisG leu2::hisG/LEU2 trp1::hisG/TRP1*	Taheri *et al.* (2000)
RH2450	**a**/α *bud9Δ::HIS3/bud9Δ::HIS3 his3::hisG/his3::hisG ura3-52/ura3-52 TRP1/trp1::hisG leu2::hisG/LEU2*	Taheri *et al.* (2000)
RH2453	**a**/α *bud8Δ::HIS3/bud8Δ::HIS3 bud9Δ::HIS3/bud9Δ::HIS3 ura3-52/ura3-52 his3::hisG/his3::hisG leu2::hisG/LEU2 trp1::hisG/TRP1*	Taheri *et al.* (2000)
YHUM829	**a**/α *ura3-52/ura3-52 leu2::hisG/leu2::hisG*	This study
YHUM1424	**a**/α *bud8Δ::HIS3/bud8Δ::HIS3 ura3-52/ura3-52 his3::hisG/his3::hisG leu2::hisG/leu2::hisG trp1::hisG/TRP1*	This study
YHUM861	α *bud8Δ::HIS3 ura3-52 his3::hisG leu2::hisG*	This study
YHUM904	**a** *bud8Δ::HIS3 ura3-52 his3::hisG trp1::hisG*	This study
YHUM994	**a** *bud9Δ::HIS3 ura3-52 his3::hisG leu2::hisG trp1::hisG*	This study
YHUM995	α *bud9Δ::HIS3 ura3-52 his3::hisG leu2::hisG trp1::hisG*	This study
YHUM842	**a**/α *myc^6-BUD8-URA3/myc^6-BUD8-URA3 bud8Δ::HIS3/bud8Δ::HIS3 his3::hisG/his3::hisG leu2::hisG/LEU2 trp1::hisG/TRP1*	This study
YHUM843	**a**/α *myc^6-BUD8$^{Δ7-53}$-URA3/myc^6-BUD8$^{Δ7-53}$-URA3 bud8Δ::HIS3/bud8Δ::HIS3 his3::hisG/his3::hisG leu2::hisG/LEU2 trp1::hisG/TRP1*	This study
YHUM844	**a**/α *myc^6-BUD8$^{Δ7-114}$-URA3/myc^6-BUD8$^{Δ7-114}$-URA3 bud8Δ::HIS3/bud8Δ::HIS3 his3::hisG/his3::hisG leu2::hisG/LEU2 trp1::hisG/TRP1*	This study
YHUM848	**a**/α *myc^6-BUD8$^{Δ74-216}$-URA3/myc^6-BUD8$^{Δ74-216}$-URA3 bud8Δ::HIS3/bud8Δ::HIS3 his3::hisG/his3::hisG leu2::hisG/LEU2 trp1::hisG/TRP1*	This study
YHUM850	**a**/α *myc^6-BUD8$^{Δ173-325}$-URA3/myc^6-BUD8$^{Δ173-325}$-URA3 bud8Δ::HIS3/bud8Δ::HIS3 his3::hisG/his3::hisG leu2::hisG/LEU2 trp1::hisG/TRP1*	This study
YHUM851	**a**/α *myc^6-BUD8$^{Δ268-325}$-URA3/myc^6-BUD8$^{Δ268-325}$-URA3 bud8Δ::HIS3/bud8Δ::HIS3 his3::hisG/his3::hisG leu2::hisG/LEU2 trp1::hisG/TRP1*	This study
YHUM852	**a**/α *myc^6-BUD8$^{Δ268-417}$-URA3/myc^6-BUD8$^{Δ268-417}$-URA3 bud8Δ::HIS3/bud8Δ::HIS3 his3::hisG/his3::hisG leu2::hisG/LEU2 trp1::hisG/TRP1*	This study
YHUM854	**a**/α *myc^6-BUD8$^{Δ375-505}$-URA3/myc^6-BUD8$^{Δ375-505}$-URA3 bud8Δ::HIS3/bud8Δ::HIS3 his3::hisG/his3::hisG leu2::hisG/LEU2 trp1::hisG/TRP1*	This study
YHUM855	**a**/α *myc^6-BUD8$^{Δ468-505}$-URA3/myc^6-BUD8$^{Δ468-505}$-URA3 bud8Δ::HIS3/bud8Δ::HIS3 his3::hisG/his3::hisG leu2::hisG/LEU2 trp1::hisG/TRP1*	This study
YHUM856	**a**/α *myc^6-BUD8$^{Δ513-600}$-URA3/myc^6-BUD8$^{Δ513-600}$-URA3 bud8Δ::HIS3/bud8Δ::HIS3 his3::hisG/his3::hisG leu2::hisG/LEU2 trp1::hisG/TRP1*	This study
YHUM1009	**a**/α *myc^9-BUD9-TRP1/trp1::hisG leu2::hisG/myc^9-BUD9-LEU2 bud9Δ::HIS3/bud9Δ::HIS3 ura3-52/ura3-52 his3::hisG/his3::hisG*	This study
YHUM1010	**a**/α *myc^9-BUD9$^{Δ8-48}$-TRP1/trp1::hisG leu2::hisG/myc^9-BUD9$^{Δ8-48}$-LEU2 bud9Δ::HIS3/bud9Δ::HIS3 ura3-52/ura3-52 his3::hisG/his3::hisG*	This study
YHUM1011	**a**/α *myc^9-BUD9$^{Δ8-130}$-TRP1/trp1::hisG leu2::hisG/myc^9-BUD9$^{Δ8-130}$-LEU2 bud9Δ::HIS3/bud9Δ::HIS3 ura3-52/ura3-52 his3::hisG/his3::hisG*	This study
YHUM1013	**a**/α *myc^9-BUD9$^{Δ91-218}$-TRP1/trp1::hisG leu2::hisG/myc^9-BUD9$^{Δ91-218}$-LEU2 bud9Δ::HIS3/bud9Δ::HIS3 ura3-52/ura3-52 his3::hisG/his3::hisG*	This study
YHUM1014	**a**/α *myc^9-BUD9$^{Δ168-218}$-TRP1/trp1::hisG leu2::hisG/myc^9-BUD9$^{Δ168-218}$-LEU2 bud9Δ::HIS3/bud9Δ::HIS3 ura3-52/ura3-52 his3::hisG/his3::hisG*	This study
YHUM1015	**a**/α *myc^9-BUD9$^{Δ168-283}$-TRP1/trp1::hisG leu2::hisG/myc^9-BUD9$^{Δ168-283}$-LEU2 bud9Δ::HIS3/bud9Δ::HIS3 ura3-52/ura3-52 his3::hisG/his3::hisG*	This study
YHUM1017	**a**/α *myc^9-BUD9$^{Δ244-369}$-TRP1/trp1::hisG leu2::hisG/myc^9-BUD9$^{Δ244-369}$-LEU2 bud9Δ::HIS3/bud9Δ::HIS3 ura3-52/ura3-52 his3::hisG/his3::hisG*	This study
YHUM1019	**a**/α *myc^9-BUD9$^{Δ323-450}$-TRP1/trp1::hisG leu2::hisG/myc^9-BUD9$^{Δ323-450}$-LEU2 bud9Δ::HIS3/bud9Δ::HIS3 ura3-52/ura3-52 his3::hisG/his3::hisG*	This study
YHUM1020	**a**/α *myc^9-BUD9$^{Δ406-450}$-TRP1/trp1::hisG leu2::hisG/myc^9-BUD9$^{Δ406-450}$-LEU2 bud9Δ::HIS3/bud9Δ::HIS3 ura3-52/ura3-52 his3::hisG/his3::hisG*	This study
YHUM1021	**a**/α *myc^9-BUD9$^{Δ406-544}$-TRP1/trp1::hisG leu2::hisG/myc^9-BUD9$^{Δ406-544}$-LEU2 bud9Δ::HIS3/bud9Δ::HIS3 ura3-52/ura3-52 his3::hisG/his3::hisG*	This study
YHUM1022	**a**/α *myc^9-BUD9$^{Δ460-544}$-TRP1/trp1::hisG leu2::hisG/myc^9-BUD9$^{Δ460-544}$-LEU2 bud9Δ::HIS3/bud9Δ::HIS3 ura3-52/ura3-52 his3::hisG/his3::hisG*	This study
YHUM1023	**a**/α *bud8Δ::HIS3/BUD8 myc^6-BUD8-URA3/ura3-52 his3::hisG/his3::hisG leu2::hisG/LEU2 trp1::hisG/TRP1*	This study
YHUM1024	**a**/α *bud8Δ::HIS3/BUD8 URA3/ura3-52 his3::hisG/his3::hisG leu2::hisG/LEU2 trp1::hisG/TRP1*	This study
YHUM1026	**a**/α *bud8Δ::HIS3/BUD8 myc^6-BUD8$^{Δ173-325}$-URA3/ura3-52 his3::hisG/his3::hisG leu2::hisG/LEU2 trp1::hisG/TRP1*	This study
YHUM1027	**a**/α *bud8Δ::HIS3/BUD8 myc^6-BUD8$^{Δ268-325}$-URA3/ura3-52 his3::hisG/his3::hisG leu2::hisG/LEU2 trp1::hisG/TRP1*	This study
YHUM1028	**a**/α *bud8Δ::HIS3/BUD8 myc^6-BUD8$^{Δ268-417}$-URA3/ura3-52 his3::hisG/his3::hisG leu2::hisG/LEU2 trp1::hisG/TRP1*	This study
YHUM1029	**a**/α *bud9Δ::HIS3/BUD9 myc^9-BUD9-TRP1/trp1::hisG ura3-52/ura3-52 his3::hisG/his3::hisG leu2::hisG/LEU2*	This study
YHUM1030	**a**/α *bud9Δ::HIS3/BUD9 ura3-52/ura3-52 his3::hisG/his3::hisG leu2::hisG/LEU2 TRP1/trp1::hisG*	This study
YHUM1031	**a**/α *myc^9-BUD9$^{Δ244-369}$-TRP1/trp1::hisG bud9Δ::HIS3/BUD9 ura3-52/ura3-52 his3::hisG/his3::hisG leu2::hisG/LEU2*	This study
YHUM1433	**a**/α *myc^9-BUD9$^{Δ91-218}$-TRP1/trp1::hisG leu2::hisG/myc^9-BUD9$^{Δ91-218}$-LEU2 bud9Δ::HIS3/bud9Δ::HIS3 BUD5-GFP-kanMX/BUD5-GFP-kanMX ura3-52/ura3-52 his3::hisG/his3::hisG*	This study
YHUM1438	**a**/α *myc^6-BUD8$^{Δ74-216}$-URA3/myc^6-BUD8$^{Δ74-216}$-URA3 bud8Δ::HIS3/bud8Δ::HIS3 BUD5-GFP-kanMX/BUD5-GFP-kanMX his3::hisG/his3::hisG leu2::hisG/LEU2 trp1::hisG/TRP1*	This study
YHUM1445	**a**/α *BUD5-GFP-kanMX/BUD5-GFP-kanMX ura3-52/ura3-52 leu2::hisG/LEU2 trp1::hisG/TRP1*	This study
YHUM1446	**a**/α *bud9Δ::HIS3/bud9Δ::HIS3 BUD5-GFP-kanMX/BUD5-GFP-kanMX his3::hisG/his3::hisG ura3-52/ura3-52 TRP1/trp1::hisG leu2::hisG/LEU2*	This study
YHUM1447	**a**/α *bud8Δ::HIS3/bud8Δ::HIS3 BUD5-GFP-kanMX/BUD5-GFP-kanMX ura3-52/ura3-52 his3::hisG/his3::hisG leu2::hisG/LEU2 trp1::hisG/TRP1*	This study

Table 2. Plasmids

Plasmid	Description	Reference
pRS304	*TRP1*-marked integrative vector	Sikorski and Hieter (1989)
pRS305	*LEU2*-marked integrative vector	Sikorski and Hieter (1989)
pRS306	*URA3*-marked integrative vector	Sikorski and Hieter (1989)
pRS425	*LEU2*-marked 2 μm vector	Sikorski and Hieter (1989)
pRS426	*URA3*-marked 2 μm vector	Sikorski and Hieter (1989)
BHUM782	*BUD8p-myc*^{6}*-BUD8* in pRS306	This study
BHUM783	*BUD8p-myc*^{6}*-BUD8*$^{\Delta 7-53}$ in pRS306	This study
BHUM784	*BUD8p-myc*^{6}*-BUD8*$^{\Delta 7-114}$ in pRS306	This study
BHUM786	*BUD8p-myc*^{6}*-BUD8*$^{\Delta 74-216}$ in pRS306	This study
BHUM788	*BUD8p-myc*^{6}*-BUD8*$^{\Delta 173-325}$ in pRS306	This study
BHUM789	*BUD8p-myc*^{6}*-BUD8*$^{\Delta 268-325}$ in pRS306	This study
BHUM790	*BUD8p-myc*^{6}*-BUD8*$^{\Delta 268-417}$ in pRS306	This study
BHUM792	*BUD8p-myc*^{6}*-BUD8*$^{\Delta 375-505}$ in pRS306	This study
BHUM793	*BUD8p-myc*^{6}*-BUD8*$^{\Delta 468-505}$ in pRS306	This study
BHUM794	*BUD8p-myc*^{6}*-BUD8*$^{\Delta 513-600}$ in pRS306	This study
BHUM796	*BUD9p-myc*^{9}*-BUD9* in pRS304	This study
BHUM797	*BUD9p-myc*^{9}*-BUD9*$^{\Delta 8-48}$ in pRS304	This study
BHUM798	*BUD9p-myc*^{9}*-BUD9*$^{\Delta 8-130}$ in pRS304	This study
BHUM800	*BUD9p-myc*^{9}*-BUD9*$^{\Delta 91-218}$ in pRS304	This study
BHUM801	*BUD9p-myc*^{9}*-BUD9*$^{\Delta 168-218}$ in pRS304	This study
BHUM802	*BUD9p-myc*^{9}*-BUD9*$^{\Delta 168-283}$ in pRS304	This study
BHUM804	*BUD9p-myc*^{9}*-BUD9*$^{\Delta 244-369}$ in pRS304	This study
BHUM806	*BUD9p-myc*^{9}*-BUD9*$^{\Delta 323-450}$ in pRS304	This study
BHUM807	*BUD9p-myc*^{9}*-BUD9*$^{\Delta 406-450}$ in pRS304	This study
BHUM808	*BUD9p-myc*^{9}*-BUD9*$^{\Delta 406-544}$ in pRS304	This study
BHUM809	*BUD9p-myc*^{9}*-BUD9*$^{\Delta 460-544}$ in pRS304	This study
BHUM810	*BUD9p-myc*^{9}*-BUD9* in pRS305	This study
BHUM811	*BUD9p-myc*^{9}*-BUD9*$^{\Delta 8-48}$ in pRS305	This study
BHUM812	*BUD9p-myc*^{9}*-BUD9*$^{\Delta 8-130}$ in pRS305	This study
BHUM814	*BUD9p-myc*^{9}*-BUD9*$^{\Delta 91-130}$ in pRS305	This study
BHUM815	*BUD9p-myc*^{9}*-BUD9*$^{\Delta 168-218}$ in pRS305	This study
BHUM816	*BUD9p-myc*^{9}*-BUD9*$^{\Delta 168-283}$ in pRS305	This study
BHUM818	*BUD9p-myc*^{9}*-BUD9*$^{\Delta 244-369}$ in pRS305	This study
BHUM820	*BUD9p-myc*^{9}*-BUD9*$^{\Delta 323-450}$ in pRS305	This study
BHUM821	*BUD9p-myc*^{9}*-BUD9*$^{\Delta 406-450}$ in pRS305	This study
BHUM822	*BUD9p-myc*^{9}*-BUD9*$^{\Delta 406-544}$ in pRS305	This study
BHUM823	*BUD9p-myc*^{9}*-BUD9*$^{\Delta 460-544}$ in pRS305	This study
BHUM824	*BUD8p-GFP*$_{UV}$*-BUD8* in pRS426	This study
BHUM825	*BUD8p-GFP*$_{UV}$*-BUD8*$^{\Delta 7-53}$ in pRS426	This study
BHUM826	*BUD8p-GFP*$_{UV}$*-BUD8*$^{\Delta 7-114}$ in pRS426	This study
BHUM828	*BUD8p-GFP*$_{UV}$*-BUD8*$^{\Delta 74-216}$ in pRS426	This study
BHUM830	*BUD8p-GFP*$_{UV}$*-BUD8*$^{\Delta 173-325}$ in pRS426	This study
BHUM831	*BUD8p-GFP*$_{UV}$*-BUD8*$^{\Delta 268-325}$ in pRS426	This study
BHUM832	*BUD8p-GFP*$_{UV}$*-BUD8*$^{\Delta 268-417}$ in pRS426	This study
BHUM834	*BUD8p-GFP*$_{UV}$*-BUD8*$^{\Delta 375-505}$ in pRS426	This study
BHUM835	*BUD8p-GFP*$_{UV}$*-BUD8*$^{\Delta 468-505}$ in pRS426	This study
BHUM836	*BUD8p-GFP*$_{UV}$*-BUD8*$^{\Delta 513-600}$ in pRS426	This study
BHUM837	*BUD9p-YFP-BUD9* in pRS426	This study
BHUM838	*BUD9p-YFP-BUD9*$^{\Delta 8-48}$ in pRS426	This study
BHUM839	*BUD9p-YFP-BUD9*$^{\Delta 8-130}$ in pRS426	This study
BHUM841	*BUD9p-YFP-BUD9*$^{\Delta 91-218}$ in pRS426	This study
BHUM842	*BUD9p-YFP-BUD9*$^{\Delta 168-218}$ in pRS426	This study
BHUM843	*BUD9p-YFP-BUD9*$^{\Delta 168-283}$ in pRS426	This study
BHUM845	*BUD9p-YFP-BUD9*$^{\Delta 244-369}$ in pRS426	This study
BHUM847	*BUD9p-YFP-BUD9*$^{\Delta 323-450}$ in pRS426	This study
BHUM848	*BUD9p-YFP-BUD9*$^{\Delta 406-450}$ in pRS426	This study
BHUM849	*BUD9p-YFP-BUD9*$^{\Delta 406-544}$ in pRS426	This study
BHUM850	*BUD9p-YFP-BUD9*$^{\Delta 460-544}$ in pRS426	This study
BHUM723	*BUD8p-myc*^{6}*-BUD8* in pRS425	This study
BHUM1016	*BUD8p-myc*^{6}*-BUD8*$^{\Delta 7-53}$ in pRS425	This study
BHUM1017	*BUD8p-myc*^{6}*-BUD8*$^{\Delta 7-114}$ in pRS425	This study
BHUM1019	*BUD8p-myc*^{6}*-BUD8*$^{\Delta 74-216}$ in pRS425	This study
BHUM1021	*BUD8p-myc*^{6}*-BUD8*$^{\Delta 173-325}$ in pRS425	This study
BHUM1022	*BUD8p-myc*^{6}*-BUD8*$^{\Delta 268-325}$ in pRS425	This study
BHUM1023	*BUD8p-myc*^{6}*-BUD8*$^{\Delta 268-417}$ in pRS425	This study
BHUM1025	*BUD8p-myc*^{6}*-BUD8*$^{\Delta 375-505}$ in pRS425	This study
BHUM706	*BUD8p-myc*^{6}*-BUD8*$^{\Delta 513-600}$ in pRS425	This study
BHUM1027	*BUD9p-myc*^{9}*-BUD9* in pRS425	This study
BHUM1028	*BUD9p-myc*^{9}*-BUD9*$^{\Delta 8-48}$ in pRS425	This study
BHUM1029	*BUD9p-myc*^{9}*-BUD9*$^{\Delta 8-130}$ in pRS425	This study
BHUM1031	*BUD9p-myc*^{9}*-BUD9*$^{\Delta 91-218}$ in pRS425	This study
BHUM1033	*BUD9p-myc*^{9}*-BUD9*$^{\Delta 168-283}$ in pRS425	This study
BHUM1035	*BUD9p-myc*^{9}*-BUD9*$^{\Delta 244-369}$ in pRS425	This study
BHUM1037	*BUD9p-myc*^{9}*-BUD9*$^{\Delta 323-450}$ in pRS425	This study
BHUM1038	*BUD9p-myc*^{9}*-BUD9*$^{\Delta 406-450}$ in pRS425	This study
BHUM1040	*BUD9p-myc*^{9}*-BUD9*$^{\Delta 460-544}$ in pRS425	This study
pHP772	p*GAL1p-GST-BUD5*ΔN_{1-70}	Kang *et al.* (2004b)
pHP1301	p*GAL1p-GST-BUD5*	Kang *et al.* (2004b)
pHP1156	p*GAL1p-GST-HIS*$_6$*-RAX1*	Kang *et al.* (2004a)
pYGEX-2T	p*GAL1p-GST*	Schlenstedt *et al.* (1995)

the *YFP-BUD9* fragment. Plasmid DNA was isolated from Ura$^+$ transformants and analyzed by PCR and DNA sequencing to obtain plasmids BHUM837 and BHUM841 to BHUM850.

Determination of Budding Patterns

For characterization of budding patterns, bud scars and birth scars were visualized by fluorescence microscopy. Cells were grown in liquid YPD medium at 30°C to an OD_{600} of 0.6, collected by centrifugation in conical polystyrene tubes, resuspended in 1 ml of water, sonicated to disperse clumps, and fixed for 2 h at room temperature by adding formaldehyde to 3.7%. Samples were rinsed twice with water, resuspended in 100 μl of a fresh stock of 1 mg/ml calcofluor white (Fluorescent Brightener 28; Sigma-Aldrich, St. Louis, MO), incubated for 10 min in the dark, washed three times with water, and resuspended in water. Birth scars and bud scars were visualized by fluorescence microscopy using a Zeiss Axiovert microscope (Carl Zeiss, Jena, Germany) and photographed using a Hamamatsu Orca ER digital camera and the Improvision Openlab software (Improvision, Coventry, United Kingdom). Budding patterns of diploid strains were determined by two different methods. For evaluation of early bud site selection, the position of bud scars was determined relative to the birth scar for each 100 cells with one, two, three, or four bud scars. Positions of bud scars were scored as "proximal" if located within the third of the cell centered on the birth scar side, as "equatorial" if located in the middle third of the cell, and as "distal" if located within the third of the cell most distal to the birth scar. To score budding patterns of older cells, cells with 5 to 12 bud scars were analyzed and divided into the following four classes: 1) "unipolar proximal" for cells with most bud scars at the proximal cell pole immediately adjacent to one another; 2) "unipolar distal" for cells with most bud scars at the distal cell pole immediately adjacent to one another; 3) "bipolar" for cells with at least three bud scars at the distal cell pole and at least one bud scar at the proximal pole; and 4) "random" for cells with bud scar distribution other than bipolar or unipolar. For each strain and experiment, at least 200 cells were analyzed. For haploid strains, positions of bud scars of at least 200 cells with more than four bud scars were determined, and cells were divided into either of the three classes "axial" for cells with most bud scars immediately adjacent to the previous site of cell separation, "bipolar" for cells with at least two bud scars at either cell pole, and "random" for all other distributions.

Green Fluorescent Protein (GFP) Fluorescence Microscopy

Strains harboring plasmids encoding GFP-Bud8p or YFP-Bud9p variants were individually grown to mid-log phase in liquid YNB medium as described for bud scar staining. Cells from 1 ml of the cultures were harvested by centrifugation and immediately viewed in vivo on a Zeiss Axiovert microscope by differential interference contrast microscopy and fluorescence microscopy using a GFP or YFP filter set (AHF Analysentechnik AG, Tübingen, Germany). Cells were photographed using a Hamamatsu Orca ER digital camera (Hamamatsu, Bridgewater, NJ) and the Improvision Openlab software (Improvision).

Protein Analysis

Preparation of Total Cell Extracts. Yeast cells were grown at 30°C in YPD medium or in SC medium lacking nutrients as needed to maintain various plasmids. Protein extracts were prepared from cultures grown to mid-log phase ($OD_{600} \sim 1.0$). Briefly, cells were harvested by centrifugation at 4°C and washed once with TE buffer (10 mM Tris-HCl, pH 8.0, and 1 mM EDTA, pH 8.0). After centrifugation, cells were resuspended in 280 μl of ice-cold buffer R (50 mM Tris-HCl, pH 7.5, 1 mM EDTA, pH 7.5, 50 mM dithiothreitol, 1 mM phenylmethylsulfonyl fluoride [PMSF], 0.5 mM *N*-tosyl-L-phenylalanine chloromethyl ketone [TPCK], 0.5 mM *N*-tosyl-L-lysine chloromethyl ketone [TLCK], and 0.5 mM pepstatin A). Cells were then broken by vortexing with glass beads for 10 min at 4°C. This step was followed by addition of Triton X-100 and SDS to a concentration of 2% to each sample and vortexing for 1 min. Crude lysates were then spun down for 2 min at 3000 rpm to remove glass beads and large cell debris. The supernatant was collected as total cell lysate. Two microliters of each extract were removed to determine total protein concentration using a protein assay kit (Bio-Rad, Munich, Germany). SDS sample buffer (Laemmli, 1970) was then added to each reaction, and proteins were denatured by heating for 10 min at 65°C.

Purification of Glutathione S-Transferase (GST)-Fusion Proteins. Extracts of strains expressing GST fusion proteins together with myc-tagged versions of Bud8p and Bud9p were prepared from cultures grown for 4 h to exponential growth phase in SC medium lacking nutrients as needed to maintain plasmids. Cells were harvested by centrifugation for 5 min at 3000 rpm, washed in 2% galactose solution, and transferred to SC medium containing 2% galactose. After incubation for 6 h at 30°C, cultures were chilled on ice. Cells were harvested by centrifugation at 4°C, washed once in B-buffer (50 mM HEPES, pH 7.5, 50 mM KCl, and 5 mM EDTA, pH 7.5), resuspended in 300 μl of ice-cold B-buffer containing protease inhibitors (50 mM dithiothreitol, 1 mM PMSF, 0.5 mM TPCK, 0.5 mM TLCK, and 0.5 mM pepstatin A), and transferred to 2-ml reaction tubes. Cells were broken by vortexing with glass beads at 4°C for 10 min, followed by addition of 300 μl of B-buffer plus protease inhibitors and Triton X-100 to a final concentration of 1%. Samples were mixed again by vortexing at 4°C for 1 min, followed by centrifugation for 3 min at 2000 rpm to remove glass beads and large cell debris. Ten microliters of extracts was removed to determine total protein concentration. Eighty microliters of the supernatant was transferred to a 1.5-ml reaction tube and denatured by addition of SDS sample buffer and heating for 5 min at 65°C. Then, 175 μl of the remaining extract was mixed with 800 μl of B-buffer plus protease inhibitors plus 1% Triton X-100 and 100 μl of 50% glutathione-Sepharose and incubated overnight at 4°C. Beads were repeatedly washed in B-buffer plus 0.1% Triton X-100 and collected to purify GST-fusion proteins and any associated proteins. Samples were denatured by heating at 65°C for 5 min in SDS sample buffer.

Plasma Membrane Association. Total cell lysates were prepared essentially as described previously (Harkins *et al.*, 2001), but by using the following protease inhibitors: 1 mM PMSF, 0.5 mM TPCK, 0.5 mM TLCK, 0.5 mM pepstatin A, and 0.01 mM chymostatin. Aliquots of total cell extracts were centrifuged for 1 h at 100,000 × *g* at 4°C, and the supernatant (S) and pellet (P) fractions were analyzed separately by SDS-polyacrylamide gel electrophoresis (PAGE) and immunoblotting.

Immunoblot Analysis. Equal amounts of proteins were subjected to SDS-PAGE by using 10% gels (Laemmli, 1970). Proteins were separated and then transferred to nitrocellulose membranes (Whatman Schleicher and Schuell, Dassel, Germany) by electrophoresis overnight at 30 V using a Mini-PROTEAN 3 electrophoresis system (Bio-Rad). Myc-tagged proteins as well as Cdc42p were detected using enhanced chemiluminescence technology (GE Healthcare, Little Chalfont, Buckinghamshire, United Kingdom) after incubation of membranes with monoclonal mouse anti-myc antibodies (9E10), rabbit polyclonal anti-Cdc42p antibodies (Santa Cruz Biotechnology, Santa Cruz, CA), or polyclonal anti-GST antibodies (Santa Cruz Biotechnology). Peroxidase-coupled goat anti-mouse immunoglobulin G and peroxidase-coupled goat anti-rabbit immunoglobulin G antibodies (Santa Cruz Biotechnology) were used as secondary antibodies.

RESULTS

Generation of Systematic BUD8 and BUD9 Deletion Sets and Expression in Diploid Yeast

To identify regions of *Bud8p* and *Bud9p* necessary for proper function and localization, we constructed systematic deletion sets of the *BUD8* and *BUD9* genes. Deletions were introduced in an overlapping manner, and they were based on the predicted secondary structure of the proteins. Constructs were epitope-tagged at the N termini for detection of the encoded proteins and expressed from the endogenous *BUD8* or *BUD9* promoters. All constructs were integrated as single copies in haploid *bud8*Δ or *bud9*Δ yeast strains, and resulting haploids were used to construct homozygous or heterozygous diploid mutant strains. Expression of all *BUD8* and *BUD9* deletion constructs was determined in homozygous diploids by Western blot analysis (Figure 1). The myc-tagged full-length Bud8p protein with a calculated mass of 75 kDa produced multiple signals occurring between 85 and 140 kDa (Figure 1A). Appearance of Bud8p at higher size partly results from glycosylation (Harkins *et al.*, 2001). Most of the Bud8p mutant proteins (with the exception of $Bud8p^{\Delta 375\text{-}505}$) produced multiple bands, with one band appearing in the range of the calculated molecular weight and with further bands appearing at a higher size, indicating that these variants are glycosylated. The epitope-tagged full-length Bud9p protein with a calculated weight of 75 kDa also produced several bands ranging from 80 to 130 kDa, reflecting modification of the protein by *N*- and *O*-glycosylation (Harkins *et al.*, 2001). All Bud9 mutant proteins were detectable, and in most cases (except $Bud9p^{\Delta 168\text{-}283}$), they produced one band appearing around the predicted molecular weight and further bands at higher sizes (Figure 1B). Remarkably, the variants of Bud8p and Bud9p that lack the predicted transmembrane domains ($Bud8p^{\Delta 513\text{-}600}$ and $Bud9p^{\Delta 460\text{-}544}$) still produced higher-molecular-weight bands, indicating that these proteins might still be glycosylated. However, the effects of the different deletions on *N*- and *O*-glycosylation of Bud8p and Bud9p were not further investigated in this study. In summary, all Bud8p and Bud9p mutant proteins were produced at levels that allowed further functional analysis.

Functional Analysis of BUD8

Functionality of the *BUD8* deletion variants in control of the bipolar bud site selection program was determined by measuring the budding pattern of the corresponding mutant strains. Bud scars of cells from diploid strains growing in the yeast form (YF) were stained with calcofluor, followed by a quantitative analysis of the budding patterns (Figure 2 and Table 3). Mutants were analyzed for bud site selection during the first four rounds of cell division of newborn daughter cells (Figure 2B) as well as for budding patterns developed by older mother cells with 5 to 12 bud scars (Figure 2A and Table 3). As shown previously, full deletion of *BUD8* causes a unipolar proximal budding pattern in diploid strains (Taheri *et al.*, 2000; Harkins *et al.*, 2001). A strain expressing a myc-tagged full-length version of *BUD8* instead of endogenous *BUD8* was phenotypically indistinguishable from the wild-type strain in that both produced a bipolar budding pattern in YF cells. Strains expressing truncated *BUD8* versions could be divided into three classes. A first class included three mutants ($BUD8^{\Delta 7\text{-}53}$, $BUD8^{\Delta 7\text{-}114}$, and $BUD8^{\Delta 468\text{-}505}$) that established a bipolar budding pattern (Figure 2 and Table 3). A quantitative evaluation of the positions of the first four bud scars revealed that the two strains expressing $BUD8^{\Delta 7\text{-}53}$ and $BUD8^{\Delta 7\text{-}114}$, respectively, formed their first two buds almost exclusively at the distal cell pole and only afterward started to select the proximal pole with significant frequency. In cells with four bud scars, ~70% of all these were located at the distal cell pole and 15–20% at the proximal pole. Thus, the N-terminal part of Bud8p (residues 7-114) does not seem to carry sequences required for establishment of the bipolar budding pattern. The third mutant of this bipolar class expressing $BUD8^{\Delta 468\text{-}505}$ produced a bipolar budding pattern after several rounds of cell division, but development of the pattern was distinct from

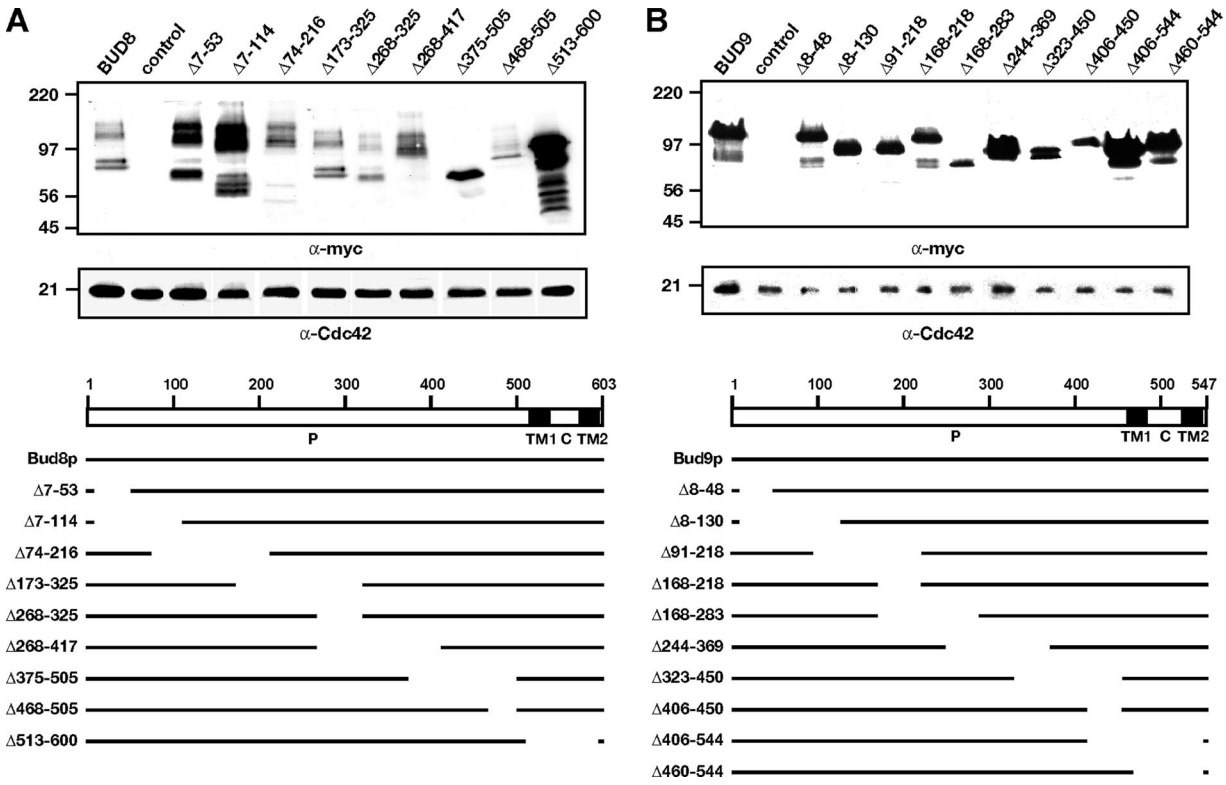

Figure 1. Expression of *BUD8* and *BUD9* constructs. (A) Expression levels of Bud8p variants. Total protein extracts were prepared from strains expressing nontagged *BUD8* (YHUM829, control), *myc*^{6}*-BUD8* (YHUM842, *BUD8*), and *myc*^{6}*-BUD8* mutant alleles (YHUM843, Δ*7-53*; YHUM844, Δ*7-114*; YHUM848, Δ*74-216*; YHUM850, Δ*173-325*; YHUM851, Δ*268-325*; YHUM852, Δ*268-417*; YHUM854, Δ*375-505*; YHUM855, Δ*468-505*; YHUM856, Δ*513-600*). Extracts were analyzed for expression of myc-epitope tagged proteins by Western blot analysis by using a monoclonal anti-myc antibody (α-myc). As an internal control, the expression of Cdc42p was measured using an anti-Cdc42p antibody (bottom). Molecular size standards (in kilodaltons) are shown on the left side. The diagram below shows the location of the two TM domains (TM1 and TM2), the predicted periplasmic (P) and cytoplasmic (C) segments, and the regions that are deleted in the different Bud8p variants. Numbers indicate amino acids residues. (B) Expression levels of Bud9p variants. Total protein extracts were prepared from a reference strain carrying the wild-type allele of *BUD9* (YHUM829), a strain carrying a *myc*^{9}*-BUD9* allele (YHUM1009, *BUD9*) and strains expressing epitope-tagged *BUD9* mutant alleles (YHUM1010, Δ*8-48*; YHUM1011, Δ*8-130*; YHUM1013, Δ*91-218*; YHUM1014, Δ*168-218*; YHUM1015, Δ*168-283*; YHUM1017, Δ*244-369*; YHUM1019, Δ*323-450*; YHUM1020, Δ*406-450*; YHUM1021, Δ*406-544*; YHUM1022, Δ*460-544*). Extracts were analyzed as described under A. The diagram shows Bud9p and Bud9p deletion variants.

that of a control strain (Figure 2 and Table 3). In the *BUD8*$^{\Delta 468\text{-}505}$ mutant strain, bud scars were formed at both cell poles with almost equal frequency already during the first rounds of cell division of newborn cells, whereas the initial bud scars of a control strain emerge predominantly from the distal pole. Thus, the Bud8p segment encompassing residues 468-505 seems to contribute to high-frequency selection of the distal pole during the first rounds of cell division of newborn cells, but it is not required for establishment of the bipolar pattern per se. The second class of mutants included three strains, which expressed the *BUD8*$^{\Delta 74\text{-}216}$, *BUD8*$^{\Delta 375\text{-}505}$, or *BUD8*$^{\Delta 513\text{-}600}$ allele. These strains predominantly selected the proximal pole for budding with very high frequency similar to a *bud8*Δ deletion strain that lacks *BUD8* (Figure 2 and Table 3). These mutants define two segments of Bud8p, one residing in the N-terminal portion and the other being located at the C-terminal part, that both are indispensable for functionality of the protein. A third class included the *BUD8*$^{\Delta 173\text{-}325}$, *BUD8*$^{\Delta 268\text{-}325}$, and *BUD8*$^{\Delta 268\text{-}417}$ expressing strains. Surprisingly, these strains produced a random budding pattern with a very high frequency ranging from 73 to 83%. A random budding phenotype has not been observed for *BUD8* mutants, except when *BUD8* is completely deleted together with *BUD9* resulting in >90% of randomly budding cells (Taheri *et al*., 2000; Harkins *et al*., 2001). We tested whether these novel variants of Bud8p were able to exert their function in the presence of the full-length Bud8 protein. For this purpose, heterozygous mutant strains were generated that carry one copy of the random allele and one copy of the regular *BUD8* gene. We found that all of these heterozygous *BUD8* mutant strains still produced a random budding pattern albeit slightly less pronounced than that observed for the corresponding homozygous mutants (Table 3), indicating that mutations of this class are dominant. Finally, expression of *BUD8*$^{\Delta 173\text{-}325}$, *BUD8*$^{\Delta 268\text{-}325}$, and *BUD8*$^{\Delta 268\text{-}417}$ in haploid strains also caused a significant increase in cells with a random budding pattern, whereas all other *BUD8* mutations did not affect haploid budding (Table 3). Thus, these variants of Bud8p might cause random budding by interfering with downstream components required for bud site selection programs of both haploids and diploids.

Functional Analysis of BUD9

The set of *BUD9* mutants was analyzed for functionality analogous to the *BUD8* mutants. A quantitative analysis of the budding patterns of YF cells was performed, and it led to the dissection of *BUD9* mutants into three functional classes. The first class includes two mutant strains carrying the *BUD9*$^{\Delta 8\text{-}48}$ or *BUD9*$^{\Delta 8\text{-}130}$ allele that encode Bud9p versions

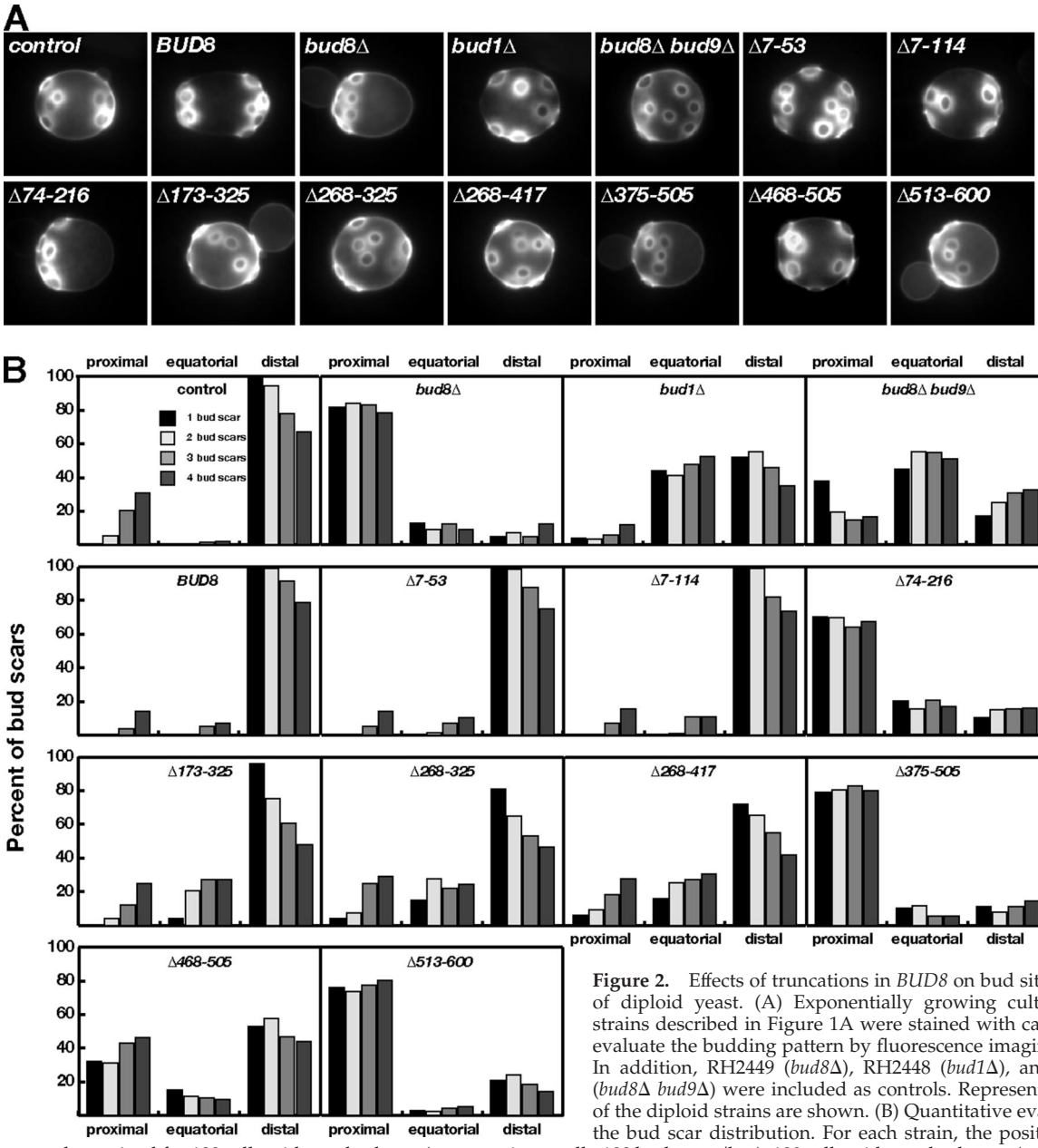

Figure 2. Effects of truncations in *BUD8* on bud site selection of diploid yeast. (A) Exponentially growing cultures from strains described in Figure 1A were stained with calcofluor to evaluate the budding pattern by fluorescence imaging of cells. In addition, RH2449 (*bud8*Δ), RH2448 (*bud1*Δ), and RH2453 (*bud8*Δ *bud9*Δ) were included as controls. Representative cells of the diploid strains are shown. (B) Quantitative evaluation of the bud scar distribution. For each strain, the positions of all bud scars were determined for 100 cells with one bud scar (representing totally 100 bud scars/bar), 100 cells with two bud scars (representing totally 200 bud scars/bar), 100 cells with three bud scars (representing totally 300 bud scars/bar), and 100 cells with four bud scars (representing totally 400 bud scars/bar). Bud scars were scored as proximal (the third making up the birth end of the cell), equatorial (the middle third of the cell located between proximal and distal cell pole), or distal (the final third that is at the pole opposite to the birth scar). Bars represent the percentage of cells at the proximal, the equatorial, and the distal region. For each strain, the average value from two independent experiments is shown.

with truncations at the N terminus. These strains established a bipolar budding pattern, and they did not significantly differ from control strains expressing the wild-type *BUD9* gene or a myc-tagged version of *BUD9* (Figure 3 and Table 3). Thus, similar to Bud8p, the N-terminal part of Bud9p (residues 8-130) is not required for establishment of the bipolar budding pattern. A second class included seven mutants carrying either the $BUD9^{\Delta 91\text{-}218}$, $BUD9^{\Delta 168\text{-}218}$, $BUD9^{\Delta 168\text{-}283}$, $BUD9^{\Delta 323\text{-}450}$, $BUD9^{\Delta 406\text{-}450}$, $BUD9^{\Delta 406\text{-}544}$, or $BUD9^{\Delta 460\text{-}544}$ allele. In these mutants, the distal cell pole was selected for budding with a high frequency similar to strains carrying a full deletion of *BUD9*. Thus, similar as in the case of Bud8p, two segments of Bud9p (one segment residing in the N-terminal half and the second segment encompassing the C-terminal region) seem to be indispensable for control of the bud site selection program by the protein. A third class of mutants was defined by a single strain expressing $BUD9^{\Delta 244\text{-}369}$, which developed a random budding pattern with a 4 to 5 times higher frequency than the control strain. This *BUD9* allele was also found to be dominant when tested in heterozygous diploid strains, indicating that the encoded Bud9p proteins might interfere with regular execution of the bipolar budding program. In haploid strains, expression of the $BUD9^{\Delta 244\text{-}369}$ did not significantly enhance random bud-

Table 3. Budding patterns[a] of *BUD8* and *BUD9* mutant strains

	Homozygous diploids				Heterozygous diploids				Haploids[b]		
	Bipolar	Unipolar proximal	Unipolar distal	Random	Bipolar	Unipolar proximal	Unipolar distal	Random	Axial	Bipolar	Random
Control	82	<0.5	8	10	nd[c]	nd	nd	nd	94	5	1
*bud8*Δ	5	89	<0.5	6	78	9	2	11	99	<0.5	<0.5
*bud9*Δ	3	<0.5	88	9	69	<0.5	23	8	95	3	2
*bud8*Δ *bud9*Δ	6	2	<0.5	92	nd	nd	nd	nd	nd	nd	nd
*bud1*Δ	2	<0.5	<0.5	97	nd	nd	nd	nd	nd	nd	nd
BUD8	70	<0.5	15	15	69	1	13	17	98	2	<0.5
Δ*7-53*	76	<0.5	10	14	nd	nd	nd	nd	96	2	2
Δ*7-114*	58	<0.5	21	21	nd	nd	nd	nd	92	7	1
Δ*74-216*	12	77	<0.5	11	nd	nd	nd	nd	nd	nd	nd
Δ*173-325*	17	1	6	76	17	<0.5	5	78	88	5	7
Δ*268-325*	24	<0.5	3	73	33	<0.5	4	63	81	7	12
Δ*268-417*	13	<0.5	4	83	32	<0.5	7	61	75	8	17
Δ*375-505*	6	85	<0.5	9	nd	nd	nd	nd	99	<0.5	<0.5
Δ*468-505*	53	28	<0.5	19	nd	nd	nd	nd	87	12	1
Δ*513-600*	5	89	<0.5	6	nd	nd	nd	nd	99	<0.5	<0.5
BUD9	76	<0.5	12	12	72	<0.5	18	10	99	<0.5	<0.5
Δ*8-48*	80	<0.5	6	14	nd	nd	nd	nd	99	<0.5	<0.5
Δ*8-130*	75	<0.5	11	14	nd	nd	nd	nd	98	1	1
Δ*91-218*	5	<0.5	86	9	nd	nd	nd	nd	98	1	1
Δ*168-218*	9	1	82	8	nd	nd	nd	nd	99	<0.5	<0.5
Δ*168-283*	11	<0.5	79	10	nd	nd	nd	nd	98	1	1
Δ*244-369*	46	<0.5	5	49	53	2	7	38	97	<0.5	3
Δ*323-450*	4	<0.5	85	11	nd	nd	nd	nd	99	<0.5	<0.5
Δ*406-450*	5	<0.5	82	13	nd	nd	nd	nd	99	<0.5	<0.5
Δ*406-544*	2	<0.5	86	12	nd	nd	nd	nd	99	<0.5	<0.5
Δ*460-544*	1	<0.5	91	8	nd	nd	nd	nd	99	<0.5	<0.5

[a] Numbers represent percentage of cells exhibiting the indicated budding pattern; values larger than 0.5 are rounded off to the next integral number.

[b] Budding patterns were determined in haploid *MAT***a** strains.

[c] Not determined.

ding. Our data indicate that as for Bud8p, distinct domains of Bud9p are involved in controlling bud site selection.

Localization of Bud8p Proteins

Subcellular localization of the different Bud8p deletion proteins was determined to identify regions of Bud8p that are necessary for a correct delivery of the protein to the distal cell pole. For this purpose, the GFP_{UV} gene was inserted between the *BUD8* promoter and the translational start site of all *BUD8* deletion alleles. Unfortunately, expression of these constructs from low-copy plasmids in diploid *bud8*Δ deletion strains did not produce signals that were sufficiently detectable by fluorescence microscopy, although the encoded fusion proteins were found to be functional when strains were assayed for budding patterns. Our previous studies have shown that expression of *GFP-BUD8* at low levels is sufficient for functional complementation but not for visual detection (Taheri *et al*., 2000). Therefore, we expressed all *GFP-BUD8* fusion genes from high-copy number plasmids, which led to a significant increase in specific fluorescent signals. Localization analysis of the different GFP-Bud8p variants in diploid *bud8*Δ strains led to three types of localization patterns (Figure 4). The full-length GFP-Bud8p and the four fusion proteins GFP-Bud8p$^{\Delta 7\text{-}53}$, GFP-Bud8p$^{\Delta 7\text{-}114}$, GFP-Bud8p$^{\Delta 74\text{-}216}$, and GFP-Bud8p$^{\Delta 468\text{-}505}$ produced a similar pattern and defined a first class. These proteins were localized on one side of unbudded cells. In small- and large-budded cells, these variants occurred at the tip of daughters and at the mother side of the bud neck (Figure 4, A–D, I, and K). These findings suggest that the N-terminal part of Bud8p does not carry signals for correct delivery of the protein to the distal cell pole. A second type of localization pattern was defined by GFP-Bud8p$^{\Delta 173\text{-}325}$, GFP-Bud8p$^{\Delta 268\text{-}325}$, and GFP-Bud8p$^{\Delta 268\text{-}417}$ that contain truncations in the median segment of Bud8p (Figure 4, E–G). These proteins were evenly distributed at the cell periphery, and they seemed to produce enhanced cytoplasmic staining, indicating that the median part of Bud8p might be required for either delivery of the proteins to polar positions or for polar maintenance after delivery. A third type of localization pattern was defined by the *GFP-BUD8*$^{\Delta 375\text{-}505}$ and *GFP-BUD8*$^{\Delta 513\text{-}600}$ fusion genes, which code for variants of Bud8p that lack the predicted C-terminal transmembrane domains or the regions immediately preceding the transmembrane (TM) domains (Figures 4, H, J, and K). These proteins seemed to be enriched in the cytoplasm, which was corroborated by crude cell fractionation of corresponding myc-epitope tagged variants showing decreased association with the plasma membrane (Figure 6). However, a significant amount of these proteins occurred as patches at the mother-daughter neck region and as dot-like structures along the cell periphery of mother and daughter cells (Figure 4), and they were still found to be associated with the plasma membrane (Figure 6). These data indicate that the C-terminal part of Bud8p is partially, but not exclusively, required for polar localization and membrane association.

Together, the N-terminal part of Bud8p does not seem to be required for correct localization, whereas segments in the

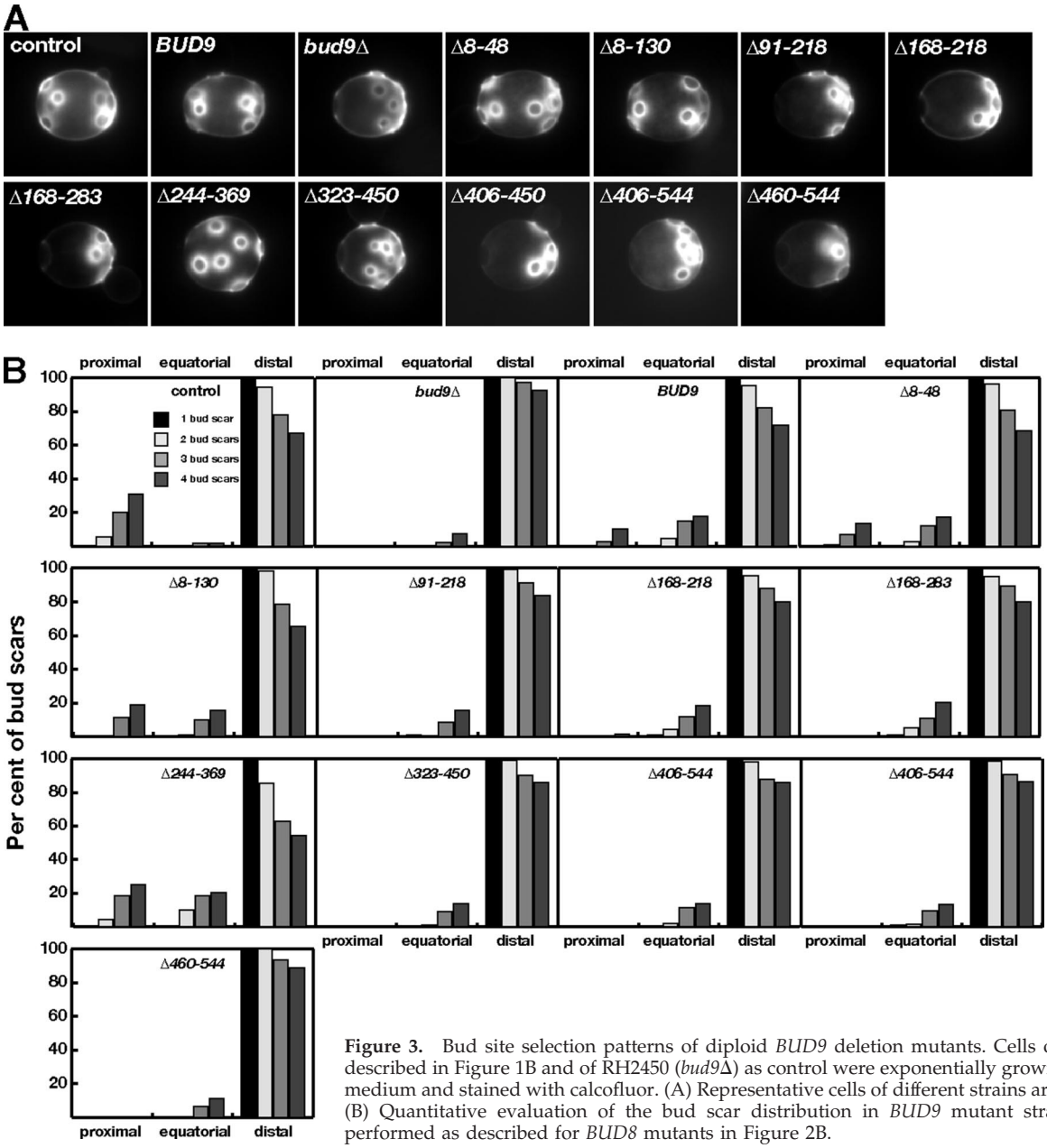

Figure 3. Bud site selection patterns of diploid *BUD9* deletion mutants. Cells of strains described in Figure 1B and of RH2450 (*bud9*Δ) as control were exponentially grown in YPD medium and stained with calcofluor. (A) Representative cells of different strains are shown. (B) Quantitative evaluation of the bud scar distribution in *BUD9* mutant strains was performed as described for *BUD8* mutants in Figure 2B.

median part and at the C terminus might be involved in delivery of the protein to the cell surface, the distal cell pole, or both.

Localization of Bud9p Proteins

Localization analysis of Bud9p mutant proteins was performed by using YFP-fusion proteins. We found that for Bud9p, expression of YFP-fusion proteins produced a considerably higher percentage of cells showing clearly detectable signals compared with GFP-fusions. *YFP-BUD9* fusions genes were expressed from the endogenous *BUD9* promoter in a *bud9*Δ strain, and the encoded YFP-Bud9p mutant proteins defined three different types of localization patterns. The full-length YFP-Bud9p control and four mutant proteins, YFP-Bud9p$^{\Delta 8\text{-}48}$, YFP-Bud9p$^{\Delta 8\text{-}130}$, YFP-Bud9p$^{\Delta 91\text{-}218}$, and YFP-Bud9p$^{\Delta 168\text{-}218}$, produced a similar localization pattern (Figure 5, A–E, and L). In unbudded cells, these proteins occurred as single patches at one or at both poles. In small-budded cells, these proteins were typically found at the tip of daughters and in mother cells at the pole opposite to the neck. In large-budded cells, proteins were found at the tip of daughters and in addition with high frequency at the mother-bud neck (see *Discussion*). All four Bud9p mutant proteins producing this type of localization pattern contain truncations in the N-terminal region, indicating that this part of the protein does not carry sequences that are essential for normal localization of Bud9p. A second type of localization pattern was defined by YFP-Bud9p$^{\Delta 168\text{-}283}$ and YFP-Bud9p$^{\Delta 244\text{-}369}$ that contain truncations in the median segment. These proteins produced highly enhanced cytoplasmic staining of cells, and polar localization was abolished (Figure 5, F, G, and L). Thus, segments lacking in these variants might be crucial for cell surface delivery. A third group of proteins included YFP-Bud9p$^{\Delta 323\text{-}450}$, YFP-

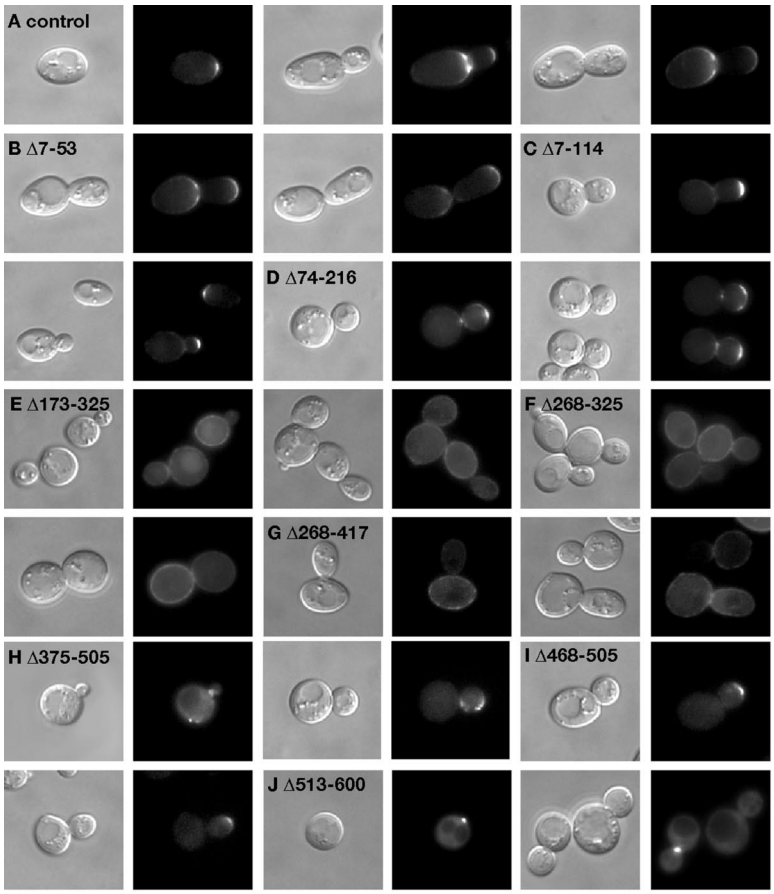

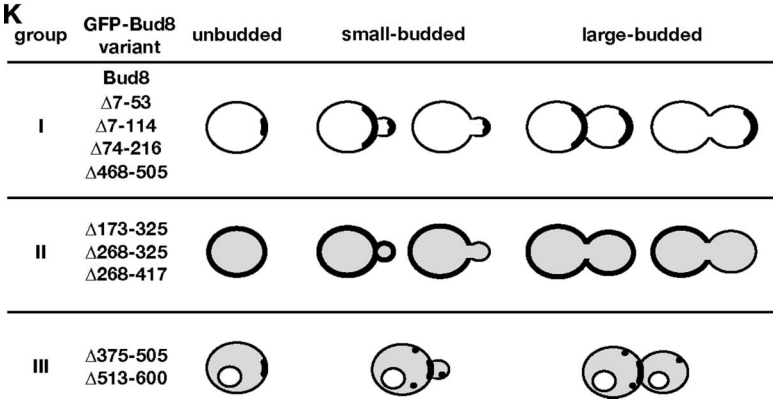

Figure 4. Subcellular localization of GFP–Bud8p mutant proteins in living cells. Representative cells of diploid *bud8*Δ*/bud8*Δ strain RH2449 expressing either full-length version of GFP–Bud8p from the plasmid BHUM824 (A) or GFP–Bud8p variants from plasmids BHUM825 (B, Δ*7-53*), BHUM826 (C, Δ*7-114*), BHUM828 (D, Δ*74-216*), BHUM830 (E, Δ*173-325*), BHUM831 (F, Δ*268-325*), BHUM832 (G, Δ*268-417*), BHUM834 (H, Δ*375-505*), BHUM835 (I, Δ*468-505*), and BHUM836 (J, Δ*513-600*), respectively, are shown. Cultures of different strains were grown overnight in YNB medium to the exponential phase, and living cells were visualized under a microscope by using Nomarski optics or fluorescence microscopy. (K) Summary of localization analysis. Shown are the most frequently observed localization patterns of GFP–Bud8p proteins at a given cell division stage (unbudded, small budded, or large budded). Single patterns shown were observed in at least 75% of stained cells ($n > 30$ cells) at a given cell division stage. Where two patterns are shown, each pattern was observed in at least 35% of cells. Depending on the localization pattern, the different GFP–Bud8p proteins were divided into different groups denoted as I to III. Black areas and black dots indicate localization of proteins at the cell periphery. Gray areas indicate putative accumulation of the proteins in the cytoplasm or at the surface, and nonstained vacuoles are shown as white spheres.

Bud9p$^{\Delta 406\text{-}450}$, YFP-Bud9p$^{\Delta 406\text{-}544}$, and YFP-Bud9p$^{\Delta 460\text{-}544}$ that lack the C-terminal TM domains or sequences immediately preceding them. These proteins produced enhanced cytoplasmic staining, which in Bud9p$^{\Delta 323\text{-}450}$ and Bud9p$^{\Delta 460\text{-}544}$ was supported by crude cell fractionation (Figures 5, H–K, and L, and 6). However, as found for Bud8 variants lacking the C-terminal segments, a fraction of these proteins still localized to the cell periphery in form of a spot at the cells tips, and was still associated with the membrane. Thus, similar to Bud8p, the C-terminal sequences of Bud9p including the two predicted TM domains are partially, but not exclusively, required for association of the protein with the cell periphery.

In summary, analysis of the different YFP-Bud9p proteins indicates that the N-terminal part of Bud9p is not required for normal localization and that segments in both the median and the C-terminal region seem to confer transport of the protein to the cell surface, to the proximal cell pole, or both.

Interaction of Bud8p and Bud9p Proteins with Bud5p and Rax1p

We further assessed putative functions of different segments of Bud8p and Bud9p by measuring physical interactions with Bud5p and Rax1p. For this purpose, we copurified Bud8p and Bud9p mutant proteins along with either GST-Bud5p or GST-Rax1p as described previously (Kang *et al.*, 2004a,b). As expected, full-length Bud8p could be copurified with GST-Bud5p (Figure 7A), but not with a variant of Bud5p lacking the N-terminal 70 amino acids (data not shown). Analysis of different Bud8p mutant proteins revealed that Bud8p$^{\Delta 74\text{-}216}$ and Bud8p$^{\Delta 375\text{-}505}$ could not be

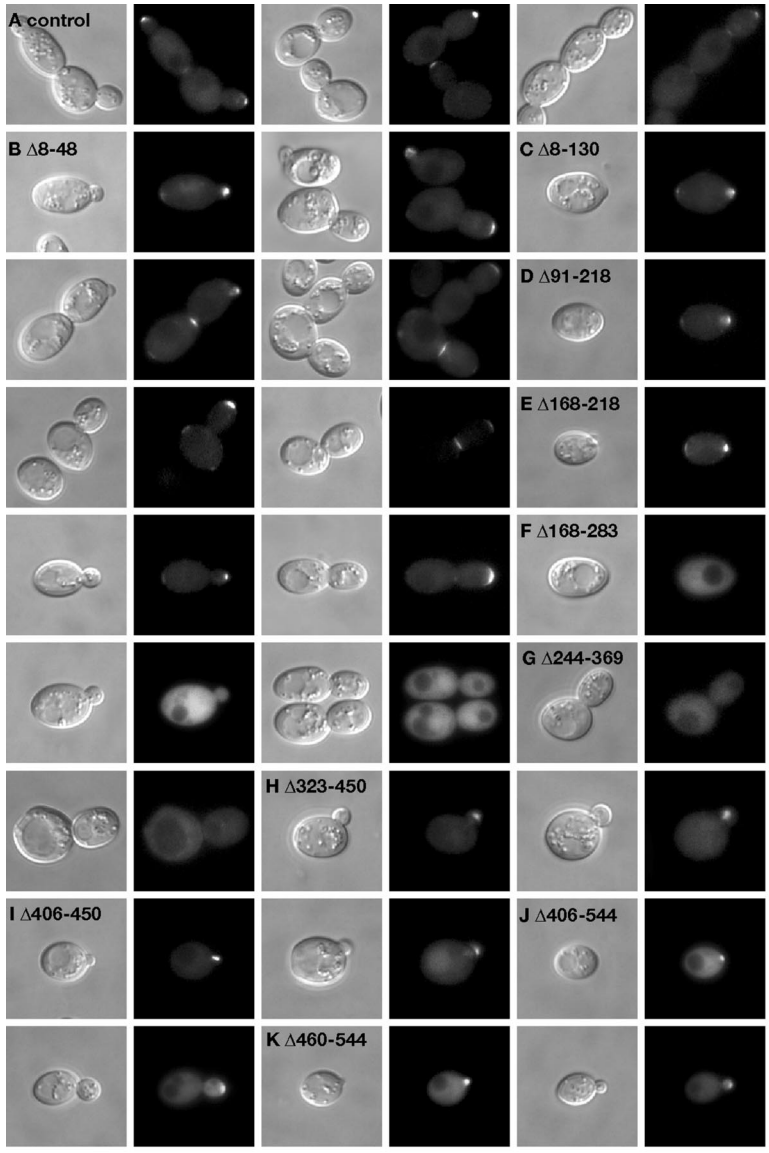

L

group	YFP-Bud9 variant	unbudded	small-budded	large-budded
I	Bud9 Δ8-48 Δ8-130 Δ91-218 Δ168-218			
II	Δ168-283 Δ244-369			
III	Δ323-450* Δ406-450* Δ406-544 Δ460-544			

Figure 5. Localization of YFP-Bud9p mutant proteins. Representative cells of diploid *bud9*Δ*/bud9*Δ strain RH2450 expressing either a full-length YFP-Bud9p protein from the plasmid BHUM837 (A) or YFP-Bud9p variants from plasmids BHUM838 (B, Δ*8-48*), BHUM839 (C, Δ*8-130*), BHUM841 (D, Δ*91-218*), BHUM842 (E, Δ*168-218*), BHUM843 (F, Δ*168-283*), BHUM845 (G, Δ*244-369*), BHUM847 (H, Δ*323-450*), BHUM848 (I, Δ*406-450*), BHUM849 (J, Δ*406-544*), and BHUM850 (K, Δ*460-544*), respectively, are shown. Cultures of corresponding strains were grown in YNB medium to the exponential phase, and living cells of different stages of the cell cycle were viewed under the microscope by using Nomarski optics or fluorescence microscopy. (L) Summary of localization analysis. Shown are the most frequently observed localization patterns of YFP–Bud9p proteins at a given cell division stage (unbudded, small budded, or large budded). Single patterns shown were observed in at least 75% of stained cells ($n > 30$ cells) at a given cell division stage. Where two patterns are shown, each pattern was observed in at least 35% of cells, and in case of three patterns, at least 20% of stained cells exhibited one of the patterns shown. Depending on the localization pattern, the different YFP–Bud9p proteins were divided into different groups denoted as I to III. Black dots and areas indicate localization of proteins at the cell periphery. Gray areas indicate putative accumulation of the proteins in the cytoplasm, and nonstained vacuoles are shown as white spheres. In Δ323-450 and Δ406-450 variants, asterisks indicate that proteins were localized predominantly in small-budded cells.

copurified with GST-Bud5p, indicating that segments deleted in these variants potentially contain sequences that confer interaction with Bud5p.

Interaction between Bud9p and Bud5p has not been demonstrated yet. Here, we found that Bud9p can be efficiently copurified with GST-Bud5p (Figure 7B) but not with GST-Bud5p$^{\Delta 1\text{-}70}$ (Figure 7C) and that binding does not require Bud8p (Figure 7C). These results indicate that the N-terminal part of Bud5p is responsible for interaction not only with Bud8p but also with Bud9p and that Bud8p and Bud9p seem to interact with Bud5p independently of each other. Analysis of deletion variants of Bud9p revealed that interaction

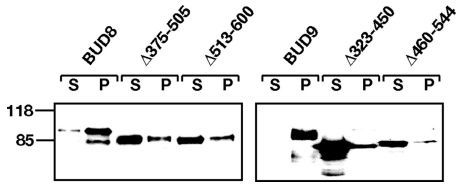

Figure 6. Plasma membrane association of Bud8p and Bud9p proteins. Total protein extracts were prepared from yeast strains YHUM842 (*BUD8*), YHUM854 (Δ*375-505*), YHUM856 (Δ*513-600*), YHUM1009 (*BUD9*), YHUM1019 (Δ*323-450*), and YHUM1022 (Δ*460-544*) and centrifuged as described in *Materials and Methods*. S and P fractions were then analyzed by immunoblotting using a monoclonal anti-myc antibody for the presence of epitope-tagged Bud8p and Bud9p proteins.

with GST-Bud5p was abolished in Bud9p$^{\Delta 91\text{-}218}$ and Bud9p$^{\Delta 168\text{-}283}$ and that it was reduced in Bud9p$^{\Delta 323\text{-}450}$ and Bud9p$^{\Delta 406\text{-}450}$ (Figure 7B), indicating that the deleted segments might confer association with Bud5p.

Although we anticipated that interactions observed between Bud5p and Bud8p or Bud9p are established within living cells, we tested whether interaction between these proteins might also occur after lysis of the cells. Therefore, we performed postlysis binding experiments by mixing a protein extract prepared from a strain only expressing GST-Bud5p with extracts from strains expressing different epitope-tagged variants of Bud8p or Bud9p. These experiments revealed no physical interactions between Bud5p and Bud8p or Bud9p (Figure 7D), indicating that physical associations observed with strains coexpressing the binding partners reflect interaction of the proteins in vivo.

It has been shown that Bud8p and Bud9p influence the localization of Bud5p in living cells (Kang *et al*., 2001). We therefore investigated, whether the N-terminal segments identified in Bud8p and Bud9p to be required for physical association with GST-Bud5p would also be involved in localization of Bud5p-GFP in living cells. For this purpose, we constructed diploid strains chromosomally expressing *BUD5-GFP* instead of the endogenous *BUD5* and carrying full deletions of either *BUD8* or *BUD9* or expressing the *BUD8*$^{\Delta 74\text{-}216}$ or *BUD9*$^{\Delta 91\text{-}218}$ variants lacking putative Bud5p interaction domains. Although these strains produced only weak Bud5p-GFP signals, specific patterns of localization could be observed. Similar to previous studies, Bud5p-GFP was found at the tip of unbudded cells and at the bud tip, bud neck, or both of large-budded cells (Figure 8). The overall pattern seemed not to be dependent on Bud8p or Bud9p. However, we found that absence of Bud8 led to a reduction of large-budded cells with Bud5-GFP being localized at the bud tip. A similar decrease was found in cells expressing *BUD8*$^{\Delta 74\text{-}216}$, but not in cells lacking *BUD9*. Vice versa, either full deletion of *BUD9* or deletion of the *BUD9* segment for residues 91-218 caused a reduction of large-budded cells having Bud5p-GFP localized at the bud neck. Thus, the Bud8p segment 74-216 and the Bud9 segment 91-218 are not only required for interaction with GST-Bud5p but also seem to affect localization of Bud5p-GFP in living cells.

Finally, we could confirm interaction of GST-Rax1p with full-length versions of Bud8p and Bud9p (Figure 9, A and B). Analysis of the mutant proteins revealed that copurification with GST-Rax1p was abolished in Bud9p$^{\Delta 168\text{-}283}$, Bud9p$^{\Delta 323\text{-}450}$, and Bud9p$^{\Delta 460\text{-}544}$, and it was clearly reduced in Bud8p$^{\Delta 7\text{-}53}$, Bud8p$^{\Delta 7\text{-}114}$, Bud8p$^{\Delta 375\text{-}505}$, and Bud8p$^{\Delta 513\text{-}600}$ (Figure 9, A and B). These experiments identify potential Rax1p interaction domains in Bud8p and Bud9p, and

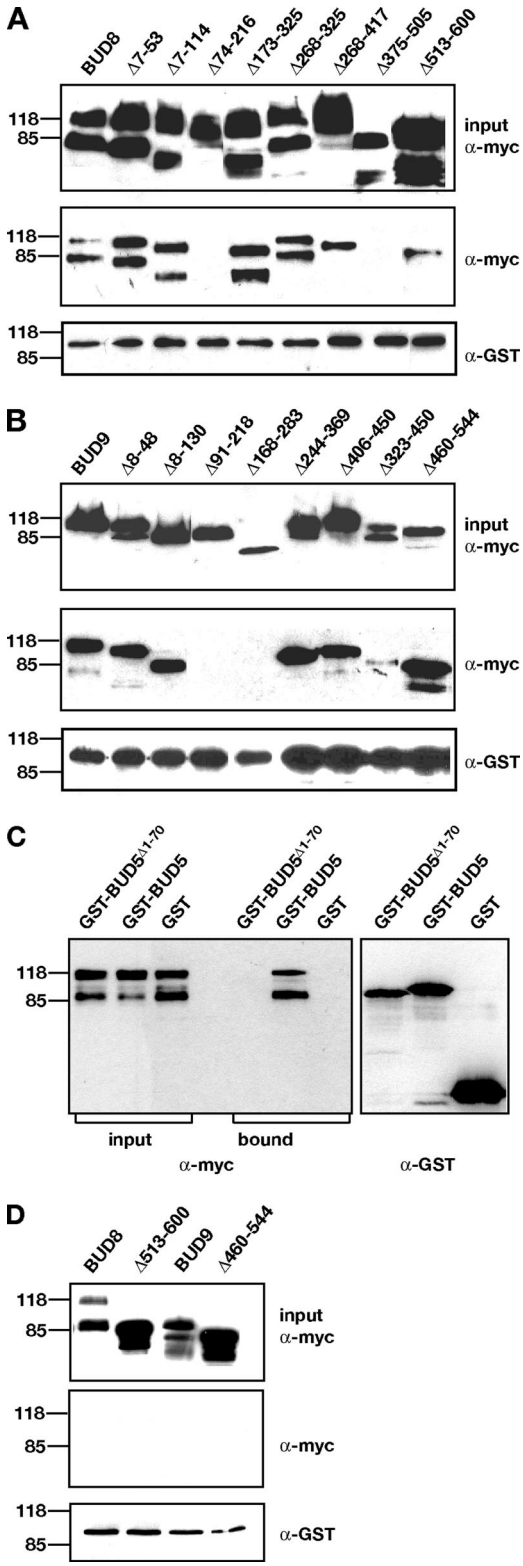

Figure 7. Interaction of Bud8p and Bud9p proteins with Bud5p. (A) Copurification of different variants of Bud8p with GST-Bud5p. Protein extracts were prepared from diploid yeast strain YHUM829 carrying plasmid pHP1301 (Kang *et al*., 2004b) and either of the plasmids BHUM723 (*BUD8*), BHUM1016 (Δ*7-53*), BHUM1017 (Δ*7-114*), BHUM1019 (Δ*74-216*), BHUM1021 (Δ*173-325*), BHUM1022 (Δ*268-325*), BHUM1023 (Δ*268-417*), BHUM1025 (Δ*375-505*), or BHUM706 (Δ*513-600*), and GST–Bud5p was pulled down with

they suggest that these domains in general are not identical to the potential Bud5p binding sites found in the cortical tags.

DISCUSSION

In this study, we have performed structure-function analyses of the yeast cortical tags Bud8p and Bud9p, because both proteins, with the exception of the predicted C-terminal transmembrane segments, lack known functional domains. Specifically, we aimed at uncovering regions of the proteins that mediate polar localization, that are responsible for interaction with the GDP/GTP exchange factor Bud5p, and that mediate association with the cortical tag protein Rax1p. We chose a strategy using systematic deletion mutations, because in many other cases this approach has been very successful in defining functional domains of poorly characterized proteins. Although deletion mutations bear a certain risk of creating global alterations of protein conformation, many domains will fold properly if neighboring sequences are removed or even if isolated from their natural context. In addition, deletions that affect only a subset of the properties of the full-length protein are likely to define functional domains. Our study uncovered a number of such mutations within Bud8p and Bud9p (Table 4) indicating that the deleted regions carry domains with specific functions and that our approach was successful.

One concern of this study might be the use of the Σ1287b strain background to analyze the localization of Bud9p. In a previous study in this genetic background, we observed GFP-Bud9p predominantly at the tips of small- and large-budded daughters and only rarely at the mother-bud neck of large-budded cells (Taheri *et al*., 2000). In another strain background, GFP-Bud9p was found to be predominantly localized at the proximal pole of unbudded cells and at the bud site of the neck in large-budded cells (Harkins *et al*., 2001; Schenkman *et al*., 2002). Here, we used functional YFP-Bud9p constructs that produced much clearer signals than GFP-Bud9p in the Σ1287b strain background and enabled us to observe the protein with much higher frequency (up to 40% of stained cells) at the proximal pole of unbudded cells and at the mother-bud neck of large-budded cells. This localization pattern of Bud9p in the Σ1287b strain background is in much better agreement with the pattern observed in the other strain background and is more consistent with the idea of Bud9p being a cortical tag for the proximal pole. Thus, our experiments using YFP-Bud9p constructs seem to be sufficiently suited to identify putative localization signals in Bud9p, even though we do not know the reason for the additional tip localization of Bud9p we routinely observe in the Σ1287b background.

An important finding of our study is that Bud9p interacts with Bud5p as has been demonstrated in Bud8p (Kang *et al*., 2004b). We have previously found that Bud8p can physically interact with Bud9p (Taheri *et al*., 2000). However, Bud8p and Bud9p seem to interact with Bud5p independently of each other, because we found that Bud8p is not required for Bud9p to associate with Bud5p. We further found that the N-terminal part of Bud5p that is required for interaction with Bud8p (Kang *et al*., 2004b) is also required for interaction with Bud9p. This finding is in good agreement with the fact that deletion of the N-terminal region of Bud5p is sufficient to cause random budding (Kang *et al*., 2004b). An important question is whether Bud8p and Bud9p contain similar segments to contact Bud5p. Among the most informative variants of Bud8p and Bud9p that we uncovered are Bud8p$^{\Delta 74\text{-}216}$ and Bud9p$^{\Delta 91\text{-}218}$ that in vivo are nonfunctional. In both cases, deletions specifically affect interaction with Bud5p, but not the polar localization of the proteins or interaction with Rax1p (Table 4 and Figure 10A). This suggests that the N-terminal regions of Bud8p and Bud9p might contain a domain that mediates interaction with Bud5p to activate the general bud site selection machinery. We noticed that these regions of Bud8p and of Bud9p carry a similar stretch of ~30 amino acids (Figure 10A). Whether and how these stretches that share >40% identical amino acids confer interaction with Bud5p remains to be determined. However, these putative Bud5p interaction domains are likely to reside in the extracellular space, because the N-terminal regions of Bud8p and Bud9p carry several conserved *N*- and *O*-glycosylation sites and because Bud8p and Bud9p are glycosylated in vivo (Harkins *et al*., 2001). Thus, our data indicate that additional factors might exist, which confer interaction of these extracellular portions of Bud8p and Bud9p with the N-terminal part of the cytoplasmically localized Bud5p (Figure 10B). Our data do not support Rax1p to fulfill this function, because these putative extracellular Bud5p-interacting segments of Bud8p and Bud9p are not required for Rax1p interaction. Thus, identification of such probably transmembrane proteins must be further addressed in future work.

It has been suggested that Bud8p and Bud9p might interact with downstream components through their conserved short cytoplasmic portions that are located between the two transmembrane domains (Harkins *et al*., 2001). Our results do not exclude this possibility, because we found that the C-terminal parts are required for functionality of the proteins. However, these regions of Bud8p and Bud9p do not seem to confer tight association with Bud5p, because deletion does not affect complex formation with the GDP/GTP exchange factor. Interaction of variants lacking these regions with Bud5p is likely to be established in vivo, because they do not occur postlysis and because we found that these proteins, although with reduced efficiency, are associated with the membrane and the cell periphery and that they can undergo posttranslational modification. Thus, the C-terminal regions of Bud8p and Bud9p containing the two predicted TM domains might perform their essential function

Figure 7 (cont). glutathione-Sepharose. Presence of Bud8p proteins in cell extracts (input) and after GST-Bud5p pull downs was analyzed by immunoblotting with the anti-myc antibody (α-myc), and GST-Bud5p was detected using antibodies against GST (α-GST). (B) Copurification of different variants of Bud9p with GST-Bud5p was analyzed using diploid yeast strain YHUM829 carrying plasmid pHP1301 and either of the plasmids BHUM1027 (*BUD9*), BHUM1028 (Δ*8-48*), BHUM1029 (Δ*8-130*), BHUM1031 (Δ*91-218*), BHUM1033 (Δ*168-283*), BHUM1035 (Δ*244-369*), BHUM1038 (Δ*406-450*), BHUM1037 (Δ*323-450*), or BHUM1040 (Δ*460-544*). (C) Copurification of Bud9p with different variants of Bud5p in the absence of Bud8p was analyzed in the diploid *bud8*Δ strain YHUM1424 carrying the plasmid BHUM1027 (*BUD9*) in combination with either of the plasmids pHP772 (*GST-BUD5*$^{\Delta 1\text{-}70}$), pHP1301 (*GST-BUD5*), or pYGEX-2T (*GST*). (D) Copurification of Bud8p and Bud9p proteins with Bud5p after lysis. Protein extract prepared from diploid yeast strain YHUM1424 carrying pHP1301 (GST–Bud5p) was mixed with protein extracts prepared from YHUM1424 carrying either of the plasmids BHUM723 (*BUD8*), BHUM706 (Δ*513-600*), BHUM1027 (*BUD9*), or BHUM1040 (Δ*460-544*), and GST–Bud5p was pulled down with glutathione-Sepharose. Presence of Bud8p and Bud9p proteins in cell extracts (input) and after GST–Bud5p pull downs was analyzed by immunoblotting with the anti-myc antibody (α-myc), and GST-Bud5p was detected using antibodies against GST (α-GST).

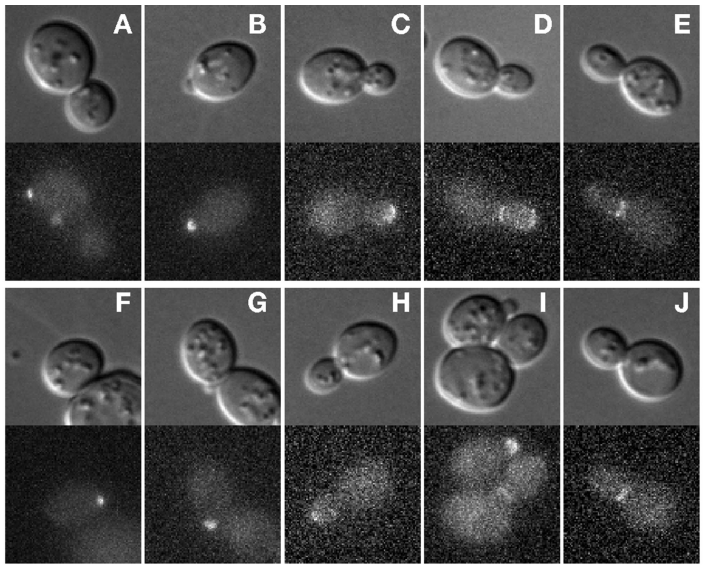

K

Bud5-GFP pattern	control	*bud8*Δ	*bud8*Δ*74-216*	*bud9*Δ	*bud9*Δ*91-218*
	26	31	29	29	32
	6	4	6	4	3
	18	19	17	21	17
	9	15	16	9	13
	24	9	11	28	27
	5	3	3	4	3
	11	17	15	3	4
other	1	2	3	2	1

Figure 8. Subcellular localization of Bud5p-GFP. Representative cells of diploid strains expressing Bud5p-GFP are shown. (A, D, E, F, G, and I) YHUM 1445 (control). (B) YHUM1447 (*bud8*Δ). (C) YHUM1446 (*bud9*Δ). (H) YHUM1433 (*bud9*Δ*91-218*). (J) YHUM1438 (*bud8*Δ*74-216*). Cultures of different strains were grown overnight in YNB medium to the exponential phase, and living cells were visualized by fluorescence microscopy. (K) Quantification. Shown are the different localization patterns found for Bud5p–GFP and the percentage of cells exhibiting these patterns for each of the strains mentioned above ($n > 300$ cells).

by, for example, transient interaction with Bud5p, or, alternatively, by interaction with other components of the general bud site selection machinery. Our study further indicates that the C-terminal regions of Bud8p and Bud9p might also be involved in transport of the proteins to the cell surface, because their deletion reduces membrane association and polar localization of the landmarks. Interestingly, deletion of the TM domains in either of the proteins not only decreases membrane association but also interaction with Rax1p. The C-terminal parts of Bud8p and Bud9p that carry the predicted TM domains show a high degree of similarity, and they are functionally interchangeable (Schenkman *et al*., 2002). Thus, correct cell surface transport of Bud8p and Bud9p might partially depend on signals present in their C-terminal regions and might involve association with Rax1p (see also discussion below).

It has been suggested that Bud8p and Bud9p are delivered to the cell surface in vesicles of the secretory system (Schenkman *et al*., 2002). However, classical N-terminal signal sequences are absent in Bud8p and Bud9p, suggesting that other parts of the proteins must confer entry into the secretory pathway. In agreement with this notion, we found that the N-terminal portions of Bud8p (residues 7-216) and of Bud9p (residues 8-218) are not required for polar localization and functionality of the proteins. We further found that most of the deletion variants produced one or several higher-molecular-weight bands in denaturing gels, indicating that these proteins are glycosylated and that they are transported through the secretory pathway. The only exceptions were the Bud8pΔ375-505 and Bud9pΔ168-283 variants that produced only one major band and that were found to be nonfunctional, indicating that these variants might not be glycosylated and therefore might lack important secretion signals. However, whether and how exactly these portions of Bud8p and Bud9p affect entry, transport, or both through the secretory system needs to be investigated in more detailed studies. In addition, future studies must reveal the exact function of glycosylation of the bipolar landmarks by,

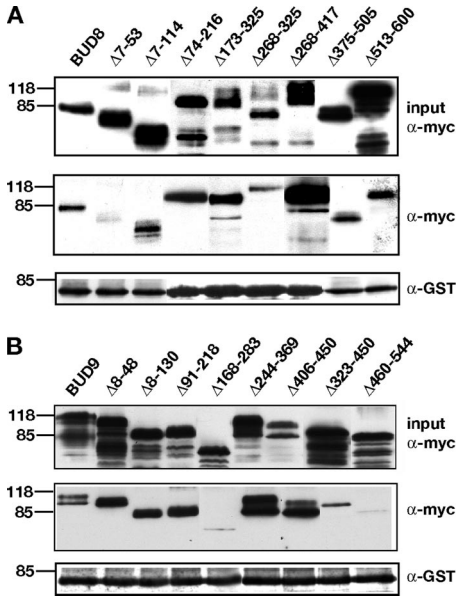

Figure 9. Interaction of Bud8p (A) and Bud9p (B) proteins with Rax1p was analyzed in diploid yeast strains carrying plasmid pHP1156 (Kang *et al.*, 2004a) and either one of the plasmids expressing different variants of *BUD8* or *BUD9* as described in Figure 6.

for example, mutational analysis of the numerous conserved *N*- and *O*-glycosylation sites present in the N-terminal portion of the proteins (Harkins *et al.*, 2001).

A further novel finding of this study is the uncovering of dominant inactive versions of *BUD8* and *BUD9* that lack the median part and that cause increased random budding. In Bud8p, the encoded mutant proteins are uniformly localized at the cell surface, indicating that they are either randomly delivered to the plasma membrane, freely diffuse in the membrane after polar delivery, or are randomly endocytosed. Our data do not allow distinguishing between these possibilities, but they suggest that the median part of Bud8p does not carry sequences essential for cell surface delivery. In addition, the median part does not seem to confer interaction with the general budding machinery, because deletions within this segment do not block interaction with Bud5p. Instead, these mutations cause dominant random budding, which might be caused by the uniformed distribution of mutant proteins on the plasma membrane making all cell cortexes competent for Bud5p binding and budding. In the case of Bud9p, deletions in the median part of the protein (Δ168-283 and Δ244-369) caused Bud9p to become enriched in the cytoplasm but not on the cell surface. The Δ168-283 deletion also abolishes interaction with Bud5p and Rax1p, which could be explained by the cytoplasmic localization of this variant (see discussion above). The Δ244-369 deletion mutant was also enriched in the cytoplasm, but it seems to be partially functional, as bipolar budding was observed in ~50% of mutant cells and as this variant was still competent for binding to Bud5p and Rax1p. Thus, in the case of Bud8p the median segments could be responsible for polar anchoring of the protein after surface delivery, whereas the median part of Bud9p seems to be involved in transport to the cell surface. Although our analysis of Bud8p and Bud9p variants lacking the median parts indicates an important role of these domains in either cell surface transport or polar anchoring, future detailed transport and localization studies are required to resolve these issues in greater detail.

Table 4. Summary of properties of different *BUD8* and *BUD9* variants and encoded proteins

	Diploid budding pattern				
	Homozygous	Heterozygous[a]	Protein localization	Bud5p interaction	Rax1p interaction
bud8Δ	Unipolar proximal	Bipolar			
BUD8	Bipolar	Bipolar	wt[b]	+	+
Δ*7-53*	Bipolar	nd[c]	wt-like	+	+/−
Δ*7-114*	Bipolar	nd	wt-like	+	+/−
Δ*74-216*	Unipolar proximal	nd	wt-like	−	+
Δ*173-325*	Random	Random	Cell periphery, cytoplasm	+	+
Δ*268-325*	Random	Random	Cell periphery, cytoplasm	+	+
Δ*268-417*	Random	Random	Cell periphery, cytoplasm	+	+
Δ*375-505*	Unipolar proximal	nd	Cell periphery and tip, neck region, cytoplasm	−	+/−
Δ*468-505*	Bipolar/random	nd	wt-like	nd	nd
Δ*513-600*	Unipolar proximal	nd	Cell periphery and tip, neck region, cytoplasm	+	+/−
bud9Δ	Unipolar distal	Bipolar			
BUD9	Bipolar	Bipolar	wt	+	+
Δ*8-48*	Bipolar	nd	wt-like	+	+
Δ*8-130*	Bipolar	nd	wt-like	+	+
Δ*91-218*	Unipolar distal	nd	wt-like	−	+
Δ*168-218*	Unipolar distal	nd	wt-like	nd	nd
Δ*168-283*	Unipolar distal	nd	Cytoplasm	−	−
Δ*244-369*	Bipolar/random	Bipolar/random	Cytoplasm	+	+
Δ*323-450*	Unipolar distal	nd	Cytoplasm, tip of daughters	+/−	+/−
Δ*406-450*	Unipolar distal	nd	Cytoplasm, tip of daughters	+/−	+
Δ*406-544*	Unipolar distal	nd	Cytoplasm, tip of daughters	nd	nd
Δ*460-544*	Unipolar distal	nd	Cytoplasm, tip of daughters	+	−

[a] In combination with *BUD8* (*BUD8* variants) or *BUD9* (*BUD9* variants).

[b] Wild type.

[c] Not determined.

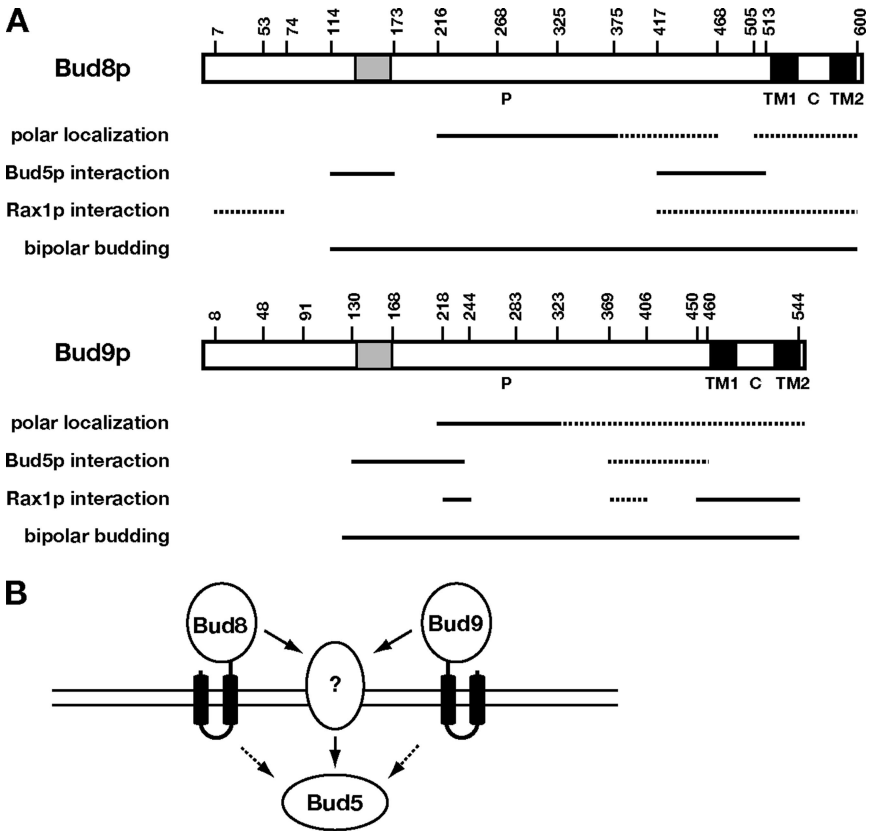

Figure 10. (A) Regions of Bud8p and Bud9p required for polar localization, Bud5p and Rax1p interaction, and bipolar budding. Numbers indicate amino acid residues that mark the borders of the various deletion constructs. Solid lines indicate full requirements and dotted lines partial requirements. Predicted P and C regions are indicated, transmembrane domains (TM1 and TM2) are shown in black, and the short N-terminal stretches sharing 40% identical amino acids (Bud8p, residues 119-166 and Bud9p, residues 132-168) are shown in gray. (B) Model for interaction of Bud8p and Bud9p with Bud5p at the plasma membrane (for details, see text).

Finally, our study has uncovered several Bud8p and Bud9p mutants defective for interaction with the cortical tag protein Rax1p. In Bud8p, we uncovered sequences in the N-terminal (Δ7-53 and Δ7-114) and the C-terminal (Δ375-505 and Δ513-600) parts that are required for efficient Rax1 binding (Figure 10A). In the C-terminal deletions, loss of Rax1p binding might be due to cytoplasmic mislocalization of the proteins. However, variants lacking N-terminal sequences are normally localized, suggesting that loss of Rax1p binding is not caused by mislocalization. Interestingly, these variants are fully functional with respect to bud site selection, indicating that the Bud8p-Rax1p interaction is not essential for functionality or polar localization of Bud8p, a conclusion that is in agreement with the previous finding that GFP-Bud8p localization does not depend on Rax1p (Kang *et al*., 2004a). Thus, although it is interesting to note that the N-terminal region of Bud8p might have a specific function in Rax1p binding, the role of the Bud8p-Rax1p interaction remains elusive. In Bud9p, is has been shown that deletion of Rax1p causes Bud9p to be mislocalized (Kang *et al*., 2004a). Here, we observed a correlation between transport of the protein to the cell surface and Rax1p binding, because the three mutations that strongly affect Rax1p binding (Δ168-283, Δ323-450, and Δ460-544) also induce cytoplasmic staining of Bud9p. In all cases, cytoplasmic localization might prevent interaction of the proteins with Rax1p. Thus, although our study has not identified a specific Rax1p-binding domain in Bud9p, it suggests that interaction of Bud9p and Rax1p depends on regular transport of these transmembrane glycoproteins to the cell surface.

In conclusion, our study has identified domains within Bud8p and Bud9p that seem to be involved in delivery of the proteins to the cell surface and to polar sites that are likely to confer interaction with components of the general budding machinery and that seem to mediate interaction with other components of the bipolar landmarks. As such, the study aids in extending our still limited knowledge on the structure and function of these cortical tag proteins and helps to better understand how these transmembrane glycoproteins participate in spatial control of cell division.

ACKNOWLEDGMENTS

We thank Hay-Oak Park (Ohio State University) for generous gifts of plasmids and strains and Gerhard Braus and Sven Krappmann for fruitful discussions. We are grateful to Diana Howey, Inken Wollenweber, and Christof Taxis for help with some of the experiments and to Maria Meyer and Diana Kruhl for technical assistance. This work was supported by grants from the Deutsche Forschungsgemeinschaft.

REFERENCES

Bauer, F., Urdaci, M., Aigle, M., and Crouzet, M. (1993). Alteration of a yeast SH3 protein leads to conditional viability with defects in cytoskeletal and budding patterns. Mol. Cell. Biol. *13*, 5070–5084.

Chant, J. (1999). Cell polarity in yeast. Annu. Rev. Cell Dev. Biol. *15*, 365–391.

Chant, J., and Herskowitz, I. (1991). Genetic control of bud site selection in yeast by a set of gene products that constitute a morphogenetic pathway. Cell *65*, 1203–1212.

Chant, J., and Pringle, J. R. (1995). Patterns of bud-site selection in the yeast *Saccharomyces cerevisiae*. J. Cell Biol. *129*, 751–765.

Chen, T., Hiroko, T., Chaudhuri, A., Inose, F., Lord, M., Tanaka, S., Chant, J., and Fujita, A. (2000). Multigenerational cortical inheritance of the Rax2 protein in orienting polarity and division in yeast. Science *290*, 1975–1978.

Drubin, D. G., and Nelson, W. J. (1996). Origins of cell polarity. Cell *84*, 335–344.

Freifelder, D. (1960). Bud position in *Saccharomyces cerevisiae*. J. Bacteriol. *80*, 567–568.

Fujita, A., Oka, C., Arikawa, Y., Katagai, T., Tonouchi, A., Kuhara, S., and Misumi, Y. (1994). A yeast gene necessary for bud-site selection encodes a protein similar to insulin-degrading enzymes. Nature *372*, 567–570.

Guthrie, C., and Fink, G. R. (1991). Guide to Yeast Genetics and Molecular Biology, San Diego, CA: Academic Press.

Harkins, H. A., Page, N., Schenkman, L. R., De Virgilio, C., Shaw, S., Bussey, H., and Pringle, J. R. (2001). Bud8p and Bud9p, proteins that may mark the sites for bipolar budding in yeast. Mol. Biol. Cell *12*, 2497–2518.

Hicks, J. B., Strathern, J. N., and Herskowitz, I. (1977). Interconversion of yeast mating types III. Action of the homothallism (*HO*) gene in cells homozygous for the mating type locus. Genetics *85*, 395–405.

Kang, P. J., Angerman, E., Nakashima, K., Pringle, J. R., and Park, H. O. (2004a). Interactions among Rax1p, Rax2p, Bud8p, and Bud9p in marking cortical sites for bipolar bud-site selection in yeast. Mol. Biol. Cell *15*, 5145–5157.

Kang, P. J., Lee, B., and Park, H. O. (2004b). Specific residues of the GDP/GTP exchange factor Bud5p are involved in establishment of the cell type-specific budding pattern in yeast. J. Biol. Chem. *279*, 27980–27985.

Kang, P. J., Sanson, A., Lee, B., and Park, H. O. (2001). A GDP/GTP exchange factor involved in linking a spatial landmark to cell polarity. Science *292*, 1376–1378.

Laemmli, U. K. (1970). Cleavage of structural proteins during the assembly of the head of bacteriophage T4. Nature *227*, 680–685.

Lord, M., Yang, M. C., Mischke, M., and Chant, J. (2000). Cell cycle programs of gene expression control morphogenetic protein localization. J. Cell Biol. *151*, 1501–1512.

Mösch, H.-U., and Fink, G. R. (1997). Dissection of filamentous growth by transposon mutagenesis in *Saccharomyces cerevisiae*. Genetics *145*, 671–684.

Ni, L., and Snyder, M. (2001). A genomic study of the bipolar bud site selection pattern in *Saccharomyces cerevisiae*. Mol. Biol. Cell *12*, 2147–2170.

Park, H. O., Bi, E., Pringle, J. R., and Herskowitz, I. (1997). Two active states of the Ras-related Bud1/Rsr1 protein bind to different effectors to determine yeast cell polarity. Proc. Natl. Acad. Sci. USA *94*, 4463–4468.

Park, H. O., Sanson, A., and Herskowitz, I. (1999). Localization of Bud2p, a GTPase-activating protein necessary for programming cell polarity in yeast to the presumptive bud site. Genes Dev. *13*, 1912–1917.

Pruyne, D., and Bretscher, A. (2000a). Polarization of cell growth in yeast. I. Establishment and maintenance of polarity states. J. Cell Sci. *113*, 365–375.

Pruyne, D., and Bretscher, A. (2000b). Polarization of cell growth in yeast. II. The role of the cortical actin cytoskeleton. J. Cell Sci. *113*, 571–585.

Sanders, S. L., and Herskowitz, I. (1996). The BUD4 protein of yeast, required for axial budding, is localized to the mother/BUD neck in a cell cycle-dependent manner. J. Cell Biol. *134*, 413–427.

Schenkman, L. R., Caruso, C., Page, N., and Pringle, J. R. (2002). The role of cell cycle-regulated expression in the localization of spatial landmark proteins in yeast. J. Cell Biol. *156*, 829–841.

Schlenstedt, G., Saavedra, C., Loeb, J. D., Cole, C. N., and Silver, P. A. (1995). The GTP-bound form of the yeast Ran/TC4 homologue blocks nuclear protein import and appearance of poly(A)+ RNA in the cytoplasm. Proc. Natl. Acad. Sci. USA *92*, 225–229.

Sheff, M. A., and Thorn, K. S. (2004). Optimized cassettes for fluorescent protein tagging in *Saccharomyces cerevisiae*. Yeast *21*, 661–670.

Sheu, Y. J., Barral, Y., and Snyder, M. (2000). Polarized growth controls cell shape and bipolar bud site selection in *Saccharomyces cerevisiae*. Mol. Cell. Biol. *20*, 5235–5247.

Sikorski, R. S., and Hieter, P. (1989). A system of shuttle vectors and yeast host strains designed for efficient manipulation of DNA in *Saccharomyces cerevisiae.* Genetics *122*, 19–27.

Taheri, N., Köhler, T., Braus, G. H., and Mösch, H.-U. (2000). Asymmetrically localized Bud8p and Bud9p proteins control yeast cell polarity and development. EMBO J. *19*, 6686–6696.

Zahner, J. E., Harkins, H. A., and Pringle, J. R. (1996). Genetic analysis of the bipolar pattern of bud site selection in the yeast *Saccharomyces cerevisiae*. Mol. Cell. Biol. *16*, 1857–1870.